

Dear Author,

Please, note that changes made to the HTML content will be added to the article before publication, but are not reflected in this PDF.

Note also that this file should not be used for submitting corrections.



ELSEVIER

Contents lists available at ScienceDirect

## Chaos, Solitons and Fractals

Nonlinear Science, and Nonequilibrium and Complex Phenomena

journal homepage: [www.elsevier.com/locate/chaos](http://www.elsevier.com/locate/chaos)

## Dynamic bifurcations on financial markets

M. Kozłowska<sup>a</sup>, M. Denys<sup>a</sup>, M. Wiliński<sup>a</sup>, G. Link<sup>a</sup>, T. Gubiec<sup>a</sup>, T.R. Werner<sup>a</sup>, R. Kutner<sup>a</sup>,  
Z.R. Struzik<sup>b,c,d,\*</sup>

<sup>a</sup> Faculty of Physics, University of Warsaw, Pasteira 5, 02–093 Warsaw, Poland<sup>b</sup> The University of Tokyo, 7-3-1 Hongo, Bunkyo-ku, Tokyo 113-0033, Japan<sup>c</sup> RIKEN Brain Science Institute, 2-1 Hirosawa, Wako-shi 351-0198, Japan<sup>d</sup> Institute of Theoretical Physics and Astrophysics, The University of Gdańsk, Wita Stwosza 57, 80–952 Gdańsk, Poland

## ARTICLE INFO

## Article history:

Received 12 November 2015

Revised 10 February 2016

Accepted 2 March 2016

Available online xxx

## PACS:

89.65.Gh

02.50.Ey

02.50.Ga

05.40.Fb

02.30.Mv

## Keywords:

Catastrophic bifurcation breakdown

Flickering phenomena

Catastrophic slowing down

Early-warning signal

Worldwide financial crisis

## ABSTRACT

We provide evidence that catastrophic bifurcation breakdowns or transitions, preceded by early warning signs such as flickering phenomena, are present on notoriously unpredictable financial markets. For this we construct robust indicators of catastrophic dynamical slowing down and apply these to identify hallmarks of dynamical catastrophic bifurcation transitions. This is done using daily closing index records for the representative examples of financial markets of small and mid to large capitalisations experiencing a speculative bubble induced by the worldwide financial crisis of 2007.

© 2016 Published by Elsevier Ltd.

## 1. Introduction

Discontinuous phase transitions in complex systems together with critical phenomena are topics of canonical importance in statistical thermodynamics [3,11,21,33,52,55]. Much as in liquid gas or magnetic systems, during the evolution of complex systems undergoing such phase transitions, one may observe catastrophic breakdowns preceded by flickering phenomenon. These types of discontinuous or critical dynamics are generic illustrations of how small changes can lead to dramatic consequences. Such regime shifts occur as a sophisticated non-trivial phenomenon caused by a catastrophic bifurcation. This means that a catastrophe or tipping

point [5,22,55] exists, at which a sudden shift of the system to a contrasting regime may occur.<sup>1</sup>

Arguably, the effects of the critical and catastrophic slowing down are the most refined indicators of whether a system is approaching a critical point or a tipping point – a tipping point being a synonym for a catastrophic threshold, located at a catastrophic bifurcation transition [6,8,9,19,39]. The problem of whether early-warning signals in the form of critical or catastrophic slowing down phenomena such as those observed in multiple physical systems [33,52] are present on financial markets was posed by Scheffer et al. [53]. Recently, an original approach was put forward by Haldane and May [20], which models banking networks as a banking ecosystem by analogy with nature's ecosystems. Such an approach can offer a valid insight into the financial sector [24,34].

\* Corresponding author. Tel.: +81356898066.

E-mail addresses: [marz.kozlowska@poczta.onet.pl](mailto:marz.kozlowska@poczta.onet.pl) (M. Kozłowska), [Mateusz.Denys@fuw.edu.pl](mailto:Mateusz.Denys@fuw.edu.pl) (M. Denys), [mwilinski@fuw.edu.pl](mailto:mwilinski@fuw.edu.pl) (M. Wiliński), [Grzegorz.Link@gmail.com](mailto:Grzegorz.Link@gmail.com) (G. Link), [Tomasz.Gubiec@fuw.edu.pl](mailto:Tomasz.Gubiec@fuw.edu.pl) (T. Gubiec), [Tomasz.Werner@fuw.edu.pl](mailto:Tomasz.Werner@fuw.edu.pl) (T.R. Werner), [Ryszard.Kutner@fuw.edu.pl](mailto:Ryszard.Kutner@fuw.edu.pl) (R. Kutner), [z.r.struzik@p.u-tokyo.ac.jp](mailto:z.r.struzik@p.u-tokyo.ac.jp), [zbi.struzik@gmail.com](mailto:zbi.struzik@gmail.com) (Z.R. Struzik).

<sup>1</sup> For instance, such sudden shifts (or jump discontinuities) of magnetization plotted versus the magnetic field were already found in critical fields, in our earlier work [32], where we studied the influence of lattice ordering on diffusion properties.

Indeed, one of the most important attainments of the catastrophe theory in the context of economics appears to be in encompassing the concept of complexity. This viewpoint has already been adopted within various economical sectors [1,4,18,51,64–66].

The classification of crises as bifurcations between a stable regime and a novel regime provides a first step towards indentifying signatures which could be used for prediction ([55] and refs. therein). Hence, the problem of the existence of tipping points in financial markets is a heavily researched area. This is because the discovery of predictability, inevitably leads to its elimination, according to one of the most fundamental financial market paradigms. This paradigm states that as a profit can be made (for instance, from predictability), the financial market gradually annihilates such an arbitrage opportunity. Yet, the complex behaviour of financial markets, together with their evolutionary character, continues to prove that it is inherently difficult to identify predictive markers. This in effect posits that such an arbitrage opportunity is routinely present on financial markets and manifested in emergent collective behaviours.

Recently, the economists Nawrocki and Vaga used nonlinear analysis of time series of returns to describe bifurcations on financial markets [56]. Our approach, presented here, is based on the linear and bilinear analysis of detrended indices of quotations. This is because in our case we describe the linear expansion of the stochastic dynamic equation in the vicinity of an equilibrium state (stable or unstable) of the system. Hence, the two approaches should be understood to be complementary. In either case, the existence of the bifurcation transition is not contrary to the above-mentioned market paradigm because, to make a definite prediction, the specific moment of transition must be known. However, such a moment is uncertain (as it is a random variable).

There is a well-known controversy, which is the prime inspiration for our work, concerning two-state transitions on financial markets. Namely, Plerou et al. [41,42] observed two-phase behaviour on financial markets by using empirical transactions and quotes within the intraday data for the 116 most actively traded US stocks during the two-year period of 1994–1995. By examining the fluctuation of volume imbalance, that is by using some conditional probability distribution of the volume imbalance, they found a change in this distribution from uni- to bimodal. This corresponds with a market shift from an equilibrium to an out-of-equilibrium state, where these two different states were interpreted as distinct phases.

In contradiction, Potters and Bouchaud [43] pointed out that the two-phase behaviour of the above-mentioned conditional distribution is a direct consequence of generic statistical properties of the volume traded, and is not a real two-phase phenomenon. In their work on the trading volume, [38] indicated that the bifurcation phenomenon is an artefact of the distribution of trade sizes, which follows a power-law distribution with an exponent belonging to the Lévy stable domain. Further, very recently, Filimonov and Sornette [14] suggested that the trend switching phenomena in financial markets considered in [44–49,58] has a spurious character. They argued that this character stems from the selection of price peaks, which imposes a condition on the statistics of price change and of trade volumes, skewing their distributions.

Nevertheless, the two-phase phenomenon was again examined in the DAX financial index in [67], using minority games and dynamic herding models. They found that this phenomenon is a significant characteristic of financial dynamics, independent of volatility clustering. Furthermore, Jiang et al. [23] observed the bifurcation phenomenon for the Hang-Seng index as non-universal and requiring specific conditions.

The principal goal of our work is to identify and describe the main empirical facts indicating the existence of possible catastrophic bifurcation transitions (CBT) in stock markets of small and

mid to large capitalisations. In this work, we consider the bifurcation phenomenon by utilizing the concept of bistability [60] and focusing our attention on the unconditional or joint properties of the catastrophic bifurcation. We further develop and evaluate a number of principal metrics associated with catastrophic bifurcation transitions. Several of them have been previously posed and considered for financial markets ([2,15,25,35,37,50,54] and refs. therein). In particular, we identify hallmarks of the catastrophic bifurcation transition by verifying relevant fundamental indicators, for WIG,<sup>2</sup> DAX, and DJIA daily speculative bubbles on the Warsaw Stock Exchange, Frankfurter Wertpapierbörse, and New York Stock Exchange. That is, we consider the stock markets' speculative bubbles during the 2007 worldwide financial crisis for, respectively, small and mid to large capitalisations (cf. Fig. 1).

We concentrate on the analysis of daily financial market data, as we consider that daily data is the most representative as it contains evidence of both the high and the low-frequency trading. That is, daily closing data has an intermediate character containing information both from the intraday trading and from the less frequent, longer-term interday trading span. In addition, because of the existence of well-known intraday patterns, detrending procedures are better established for the daily data than for the intraday case. Both the bullish and the bearish sides of the peaks considered are detrended using a generalised exponential (or Mittag-Leffler function) decorated by oscillatory behaviour (for details see Appendix A). This is because such a function better fits the peaks considered in this work than the commonly used log-periodic function [10,13,59].

The content of the paper is as follows. Section 2 is devoted to the empirical analysis of daily data originating from three typical stock markets of small, mid and large capitalisations. In Section 3, we explain how indicators arise when the system approaches a catastrophic bifurcation threshold. Section 4 contains concluding remarks. Detailed supplementary methodological considerations are presented in the appendices.

## 2. Analysis of empirical data

### 2.1. Time series and detrending

The conceptual strategy of our approach is separately to consider the deterministic components of both the trend and the drift effects, which makes viable the analysis of determinism contained in the empirical time series. We also assume that the detrending of the time series eliminates non-stationarity.

The analysis of empirical data we perform on the bubbles (peaks) of WIG, DAX and DJIA indices covers the 2007 worldwide financial crisis (cf. the erratic curves in Fig. 1(a), (b), (c)). The shapes of WIG, DAX, and DJIA peaks are strikingly similar. This suggests an underlying generic dynamical behaviour of European stock market evolution. In particular, the shape of bull markets (or booms) represented by the left-hand side of these peaks appears to be typical on stock exchanges of small to large capitalisations, as they contain very characteristic zigzags (denoted by circles). These bull markets are the principal subject of interest to us.

In order to model the deterministic long-term (multi-year) trend of these empirical bull markets – an observable long-term deterministic pattern in the empirical data caused by the herd effect,<sup>3</sup> we here use an easily interpretable relaxation function defined by Eq. (A.1), which is a solution to a dynamic equation

<sup>2</sup> The index WIG (Warszawski Indeks Giełdowy) is the main index of the Warsaw Stock Exchange, which is of a small size.

<sup>3</sup> Trend (e.g. the price trend) results from the feedback mechanism between traders and the market, which can therefore be considered to be a complex self-organizing system [27] and refs. therein.

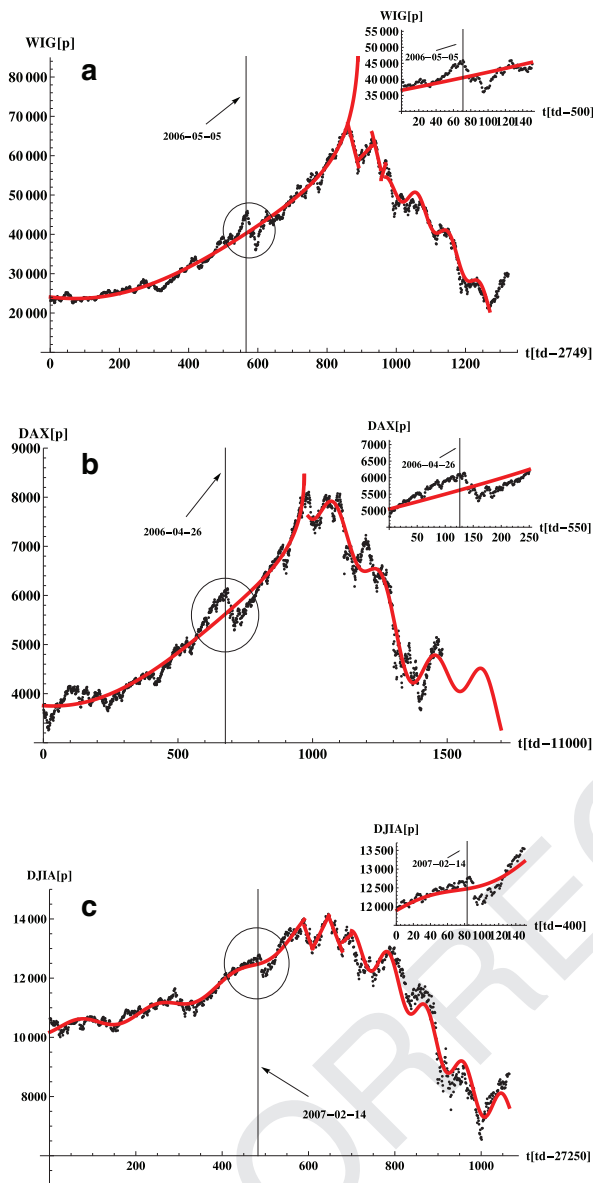


**Fig. 1.** Well-formed empirical peaks (the bubbles defined by erratic curves) of: (a) WIG index beginning on 6 February, 2004 (the -269th (=2480–2749) trading day (td) on the Warsaw Stock Exchange) and ending on 18 May, 2009 (the 1326th (=4075–2749) td), (b) DAX index beginning on 6 February, 2004 (the -269th (=2480–2749) td) trading day (td) on the Frankfurter Wertpapierbörse and ending on 18 May, 2009 (the 1326th (=4075–2749) td), and (c) DJIA index beginning on 16 March, 2005 (the 27251st td on the New York Stock Exchange) and ending on 9 June, 2009 (the 28315th td). The solid curves represent the best theoretical long-term (multi-year) trend [28], defined by Eq. (A.1), found from the fit to the bull market (left-hand side of the peak). The thin solid vertical line denotes the position of the local maximum placed for: (a) 2006-05-05 (the 576th (=3325–2749) td); (b) 26 April, 2006 (the 676th (=11676–11000) td); and (c) 14 February, 2007 (the 483rd (=27733–27250) td). These maxima belong to the zigzags marked by the circles. These zigzags are emphasized by the inset plots, as they are the main subject of interest to us. Strongly oscillating trends (also solid curves) for bear markets (the right-hand side of the peaks) are plotted only for completeness.

149 describing the relaxation of a viscoelastic market ('biopolymer') (cf. [Appendix A](#) and [29]).

150  
151 The trend and the drift each have different physical origins and  
152 operate at various time horizons, which makes their determination  
153 and analysis tractable. However, a generic problem of the decom-  
154 position of the deterministic part of time series for trend and drift  
155 components in a *unique* way is beyond the scope of this work and  
156 remains an open problem. Instead, we accept *some* level of trend

(here given, by Eq. (A.1) – see [Appendix A](#) for details) if the coefficient of determination  $R^2$  and the P-value assume the best values in comparison with the corresponding ones obtained from the fits of alternative trend functions.<sup>4</sup>

157  
158  
159  
160  
161 By subtracting the trend (A.1), we obtain the detrended time series (cf. [Fig. 2](#)) consisting of the deterministic drift and noise – the extraction of the drift component from the time series and its systematic analysis are essential for our purpose. 162  
163  
164

## 2.2. Variance of detrended time series

165  
166 For our three different time series, the time dependence of sufficiently sensitive estimators of variance, defined within the moving (or scanning) time window of one month width (or twenty trading days<sup>5</sup>) is shown in [Fig. 3](#). That is, we obtained these estimators from the corresponding separate scans of the empirical time series. These scans were made by using the above-mentioned time window of fixed width and also a fixed scanning time step (again of one trading month). Indeed, within this window the variance estimator was calculated for each temporal position of the time window. 167  
168  
169  
170  
171  
172  
173  
174  
175

176 Notably, the variance estimators of time series show a sudden strong increase in the range of downturns (marked by the circles in [Fig. 1](#)), creating local peaks of these estimators in the form of spikes (cf. three plots in [Fig. 3](#)). The centres of these spikes are indicated in the plots by the vertical dashed lines. The existence of a spike is one of the principal empirical symptoms of a catastrophic (or possibly even critical) slowing down. Henceforth in the text, we refer to these spikes as catastrophic spikes. 177  
178  
179  
180  
181  
182  
183

184 Catastrophic spikes are preceded by well-formed local peaks of variance estimators of much smaller amplitude (cf. [Fig. 3](#)). This behaviour clearly manifests the so-called flickering phenomenon [53]. This effect can happen, for instance, if the system enters the intermediate bistable (bifurcation) region placed between two tipping points. Subsequently, the system stochastically moves up and down, either between the basins of attraction of two alternative attractors, or between an attractor and a repeller. The two possibilities are defined by stable/stable or stable/unstable pairs of equilibrium states. Such behaviour can also be considered to be an early warning of catastrophe. The flickering of the variance estimator (although less intense), together with intermittencies shrinking in time, is observed for even earlier time intervals (cf. the upper plot in [Fig. 3](#)). The flickering phenomenon is considered in detail in [Sections. 2.3](#) and [2.4](#). 185  
186  
187  
188  
189  
190  
191  
192  
193  
194  
195  
196  
197  
198

## 2.3. Recovery rate

199  
200 As typical behaviour, [Fig. 4](#) plots detrended time series element or process  $x_t$  against the preceding detrended time series one,  $x_{t-1}$ , for instance, for the (detrended) time-dependent WIG index. Two plots of short (one-month) subseries of essentially different empirical data sets are shown in [Fig. 4](#) as an example. Each subseries consists of 20 successive pairs of elements ( $x_{t-1}, x_t$ ) 201  
202  
203  
204  
205

<sup>4</sup> A complementary popular candidate for the trend, also having a well-interpreted physical origin, is the log-periodic oscillation ([27] and refs. therein). However, for empirical bull markets in our data, it is worse than the fit of the trend model used by us, which has a smaller  $R^2$  (expressed, as usual, as the ratio of the explained (theoretical) variance to the sample variance). Notably,  $R^2$  is the measure of concordance most often used. Unfortunately, all hitherto known trends are nonuniversal and can be applied only to well-defined long-term bubbles. Also trends given in the form of polynomials, quite often used in econometry, result in worse statistic characteristics of the fits in our data.

<sup>5</sup> Twenty trading days is considered to be one trading month. The risk-free period of the Central Bank is likewise one month.

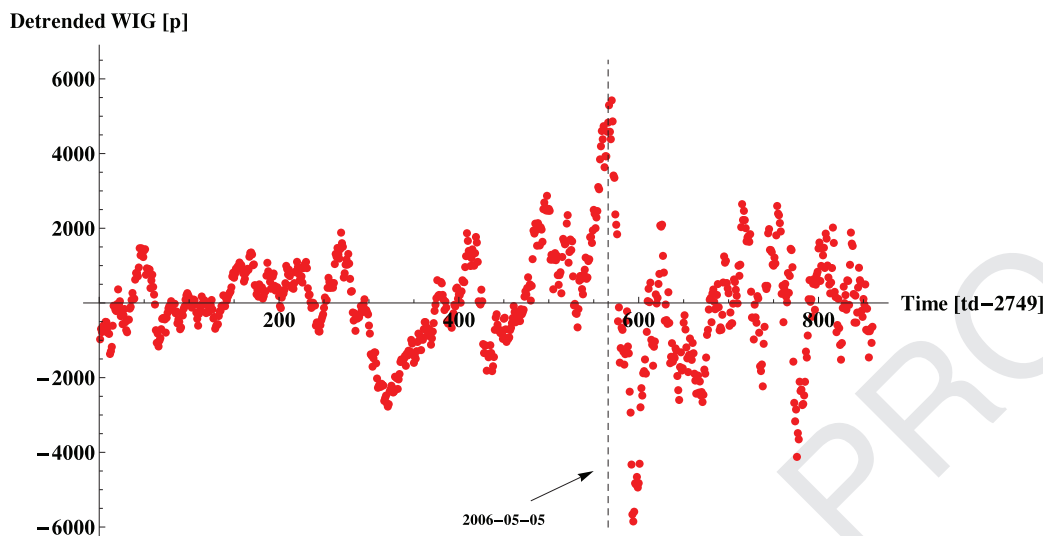


Fig. 2. The detrended time-dependent index WIG (the time series of WIG or the process  $x_t$  measured in points [p]), which constitutes the basis for further considerations. The characteristic date when the process  $x_t$  assumes its largest value is denoted by the vertical dashed line. The same date also defines the position of the index WIG's local maximum (cf. Fig. 1 (a)). The remaining indices (DAX and DJIA) show analogous behaviour and therefore, they are not presented in the figure.

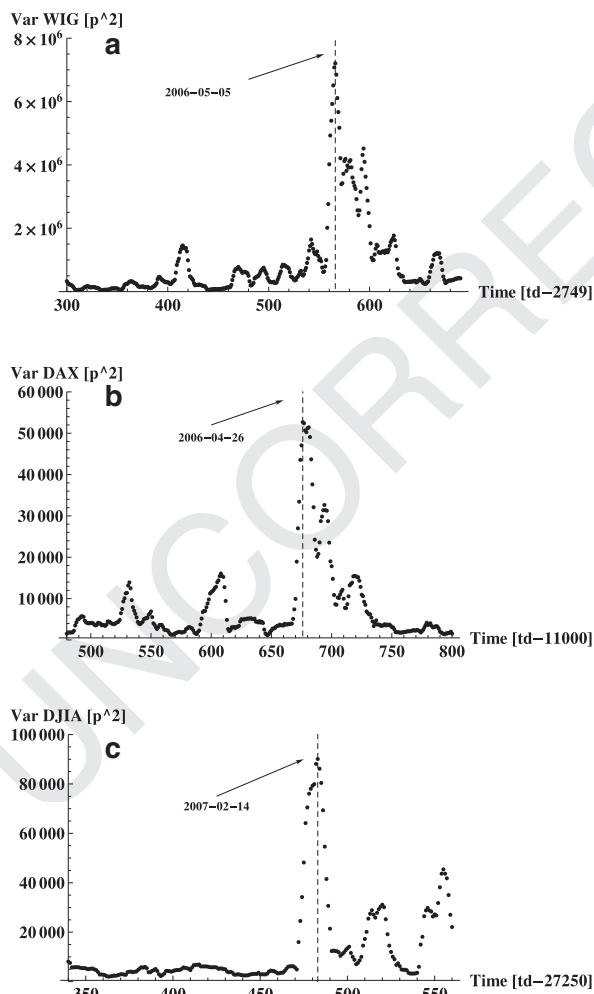


Fig. 3. Plots of the variance estimators of the detrended indices - time series of WIG, DAX and DJIA (these time series are shown in the three corresponding plots in Fig. 2). Here, the time ranges from 2005-04-15 to 2006-11-15 for WIG (plot (a)), from 2005-08-18 to 2006-10-19 for DAX (plot (b)), and from 2006-07-21 to 2007-05-09 for DJIA (plot (c)). The vertical dashed lines denote the positions of the spikes' centres.

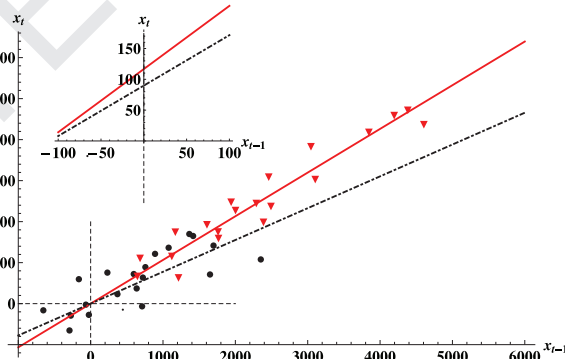
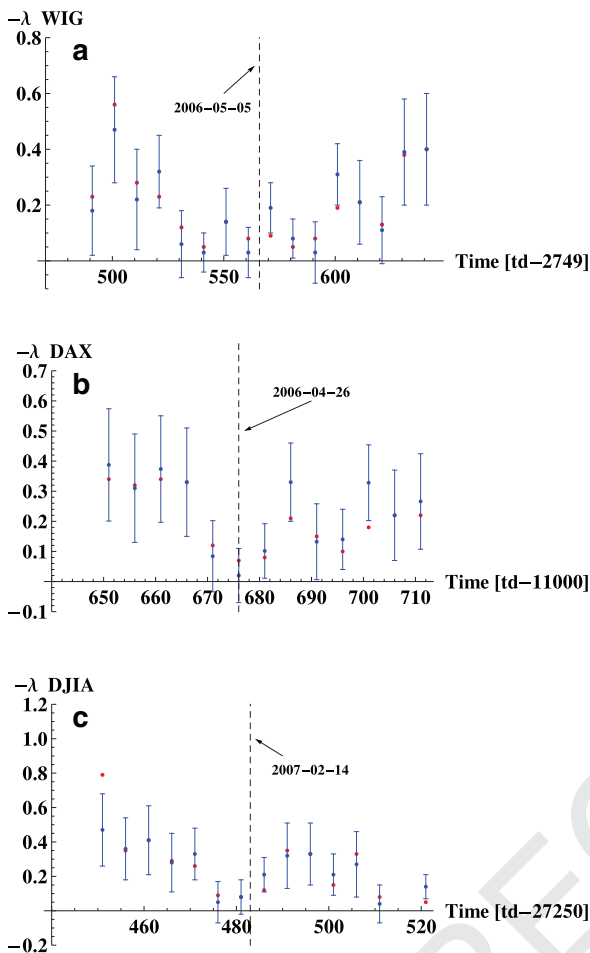


Fig. 4. The detrended successive WIG time series  $x_t$  vs.  $x_{t-1}$  for twenty pairs (or one month) ranging from  $t = 522$  to  $541$  [td-2749] (black circles and fitted black dotted-dashed straight line) and from  $t = 542$  to  $561$  [td-2749] (red inverted triangles and fitted red solid straight line) time steps. The slopes of the fitted curves, i.e. autoregressive coefficient of the first-order  $AR(1)$ , almost equal 0.65 and 0.95, respectively. These results give  $-\lambda \approx 0.35$  and  $-\lambda \approx 0.05$ , respectively. (See also plot (a) in Fig. 5.) Furthermore, respective values of the shift coefficient or autoregressive coefficient of the zero-order  $b = A(0)$ , although relatively small, are well distinguishable in the inset plot at  $x_{t-1} = 0$ . For interpretation of the references to colour in this figure legend, the reader is referred to the web version of this article.

extending from  $t = 522$  to  $t = 541$  [td-2749]<sup>6</sup> trading days (black circles) and from  $t = 542$  to  $t = 561$  [td-2749] trading days (red inverted triangles), respectively. The slopes of the straight lines, fitted separately to both data sets, give two different values of the linear or the first-order autoregression coefficient  $AR(1)$ . Hence, these slopes give values of coefficient  $\lambda = AR(1) - 1$ , where  $\lambda$  is a derivative of the nonlinear drift term,  $f(x_t; P)$  (here  $P$  is a driving or control parameter), over the time series variable,  $x_t$ , at a fixed point  $x^*$ , present in the linearized discrete stochastic dynamic Eqs. (B.6) and (B.7). This linearization is a generic property of the system which has a fixed point or contains an equilibrium (stable or unstable). These equations are valid in the vicinity of any fixed point, in particular, in the vicinity of the most interesting tipping point (or the catastrophic bifurcation threshold - cf. 206  
207  
208  
209  
210  
211  
212  
213  
214  
215  
216  
217  
218  
219

<sup>6</sup> This notation means that the origin of coordinates of plot (a) is shifted by 2749 [td] relative to the beginning of quotation on the Warsaw Stock Exchange. Analogous situations concern German Stock Exchange (plot (b)) and NYSE (plot (c))



**Fig. 5.** The recovery rate  $-\lambda (\geq 0)$  vs. time calculated by using two different formulas: (i)  $-\lambda = 1 - AR(1)$  (blue dots with error bars) and (ii)  $-\lambda = 1 - ACF(1)$  (red dots without error bars). The two curves have similar shapes in time (they are concave where data resolution equals 2 [td] to make the plots better visible) having local minima for  $-\lambda \approx 0.0$ . As these minima are reached from their positive sides, such a behaviour leads to the slowing down of the system's return to the stable equilibrium (see Appendix B for details). The vertical dashed lines denote in plots (a), (b), and (c) (as usual) the position of tipping points. For interpretation of the references to colour in this figure legend, the reader is referred to the web version of this article.

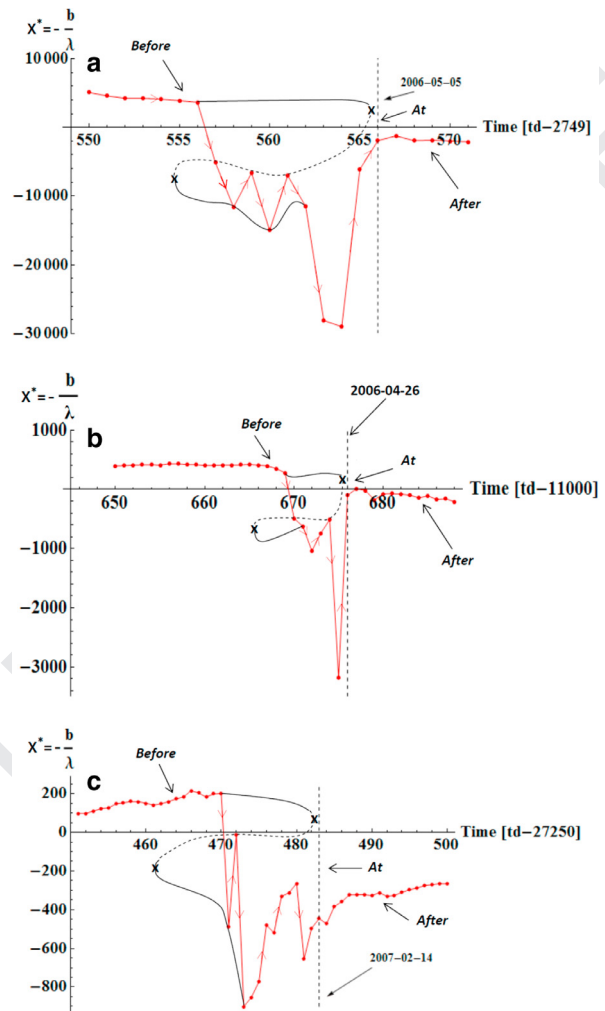


**Fig. 6.** Empirical curves (small red circles joined by the segments of red lines presented in plots (a), (b), and (c)), representing the (mechanical) equilibrium states defined by the values of  $x^* (= -b/\lambda)$  vs. time (in trading days, td), where  $b$  and  $\lambda$  were obtained from the empirical data for WIG, DAX, and DJIA (cf. Figs. 4 and 5). The flickering phenomenon, present prior to the catastrophic bifurcation threshold, is illustrated by the red curve directed by arrows which oscillate up and down between red empirical data points located alternately on the dotted and solid black curves. This threshold is marked by the dashed vertical line indicated by an arrow termed 'At'. The upper segment of the backward-folded curve is the solid one – initially red with dots and then black. It is indicated by the arrow termed 'Before' and drawn schematically until the right tipping point denoted by the character 'x' (placed one day before the catastrophic bifurcation threshold). This upper segment is identified as a sequence of stable (mechanical) equilibrium states of the type  $x_1^*$  (see Appendix C and Figs. 8–11 for details). The segment (denoted by the dotted curve) placed in the bistable region between two tipping points (the left tipping point is also denoted by the character 'x') consists of a sequence of unstable (mechanical) equilibrium states of the type  $x_2^*$  (see Appendix C and Figs. 8–11 for details). The lower segment (also denoted by the solid curve - initially black and then red) placed after the left tipping point is identified as a complementary sequence of the stable (mechanical) equilibrium states, here of  $x_1^*$  type (its part after the catastrophic bifurcation threshold is indicated by the arrow and termed 'After'; see Appendix C and Figs. 8–11 for details). Remarkably, the dotted curve can be smoothly plotted between the two tipping points and over the empirical points. (An explanation about the construction of the backward folded curve is given in paragraph 2.4). For interpretation of the references to colour in this figure legend, the reader is referred to the web version of this article.

220 Appendix B). Furthermore, different values of the shift coefficient  
 221  $b (= A(0))$ , being a zero-order autoregression coefficient), although  
 222 relatively small, are well distinguishable in the inset plot.  
 223 From the fits mentioned above,  $AR(1)$  coefficient almost equal  
 224 to 0.95 is found (cf. the slope of the red solid straight line, shown  
 225 in Fig. 4, fitted to the red inverted triangles – this corresponds to  
 226 the time interval ranging from  $t = 542$  to  $t = 561$  [td-2749] shown  
 227 in Fig. 5(a)) for the subseries containing the catastrophic bifurca-  
 228 tion threshold (marked by the dashed vertical straight lines plotted  
 229 in Figs. 2 and 3). In Fig. 5(a) this slope gives the  $-\lambda$  represented  
 230 by the blue dot with error bar placed at time  $t = 542$  [td-2749]  
 231 on the left-hand side of the catastrophic bifurcation threshold. The  
 232 black dashed straight line is shown for comparison in Fig. 4, hav-  
 233 ing a distinctly lower slope  $AR(1) \approx 0.65$ , which corresponds to the  
 234 time interval ranging from  $t = 522$  to  $t = 541$  [td-2749]. Hence, the  
 235 corresponding  $-\lambda \approx 0.35$  is represented in the same figure by the  
 236 blue dot with the error bar placed at time  $t = 522$  [td-2749], also  
 237 on the left-hand side of the catastrophic bifurcation threshold. The  
 238 origin of the red dots (without error bars) obtained using a com-  
 239plementary approach is described below.

240 In Appendix B, we prove that the autocorrelation function of  
 241 the  $h$ th order,  $ACF(h)$ , is expressed by the formula given in the  
 242 second row in (B.10). In fact, we here study a particular case of  
 243  $ACF(1) = AR(1)$  by a method complementary to that used above  
 244 for the analysis of the coefficient  $AR(1)$ . Namely, we apply the usual  
 245 estimator,  $ACF_{EST}(1)$ , of  $ACF(1)$  for a given month (which is our time

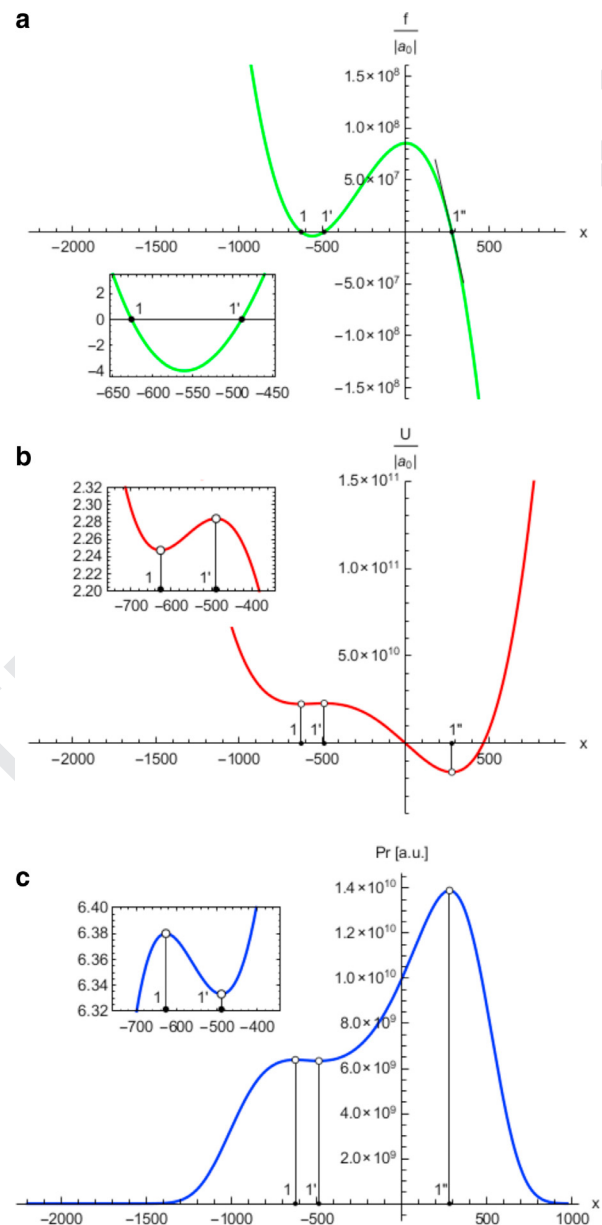
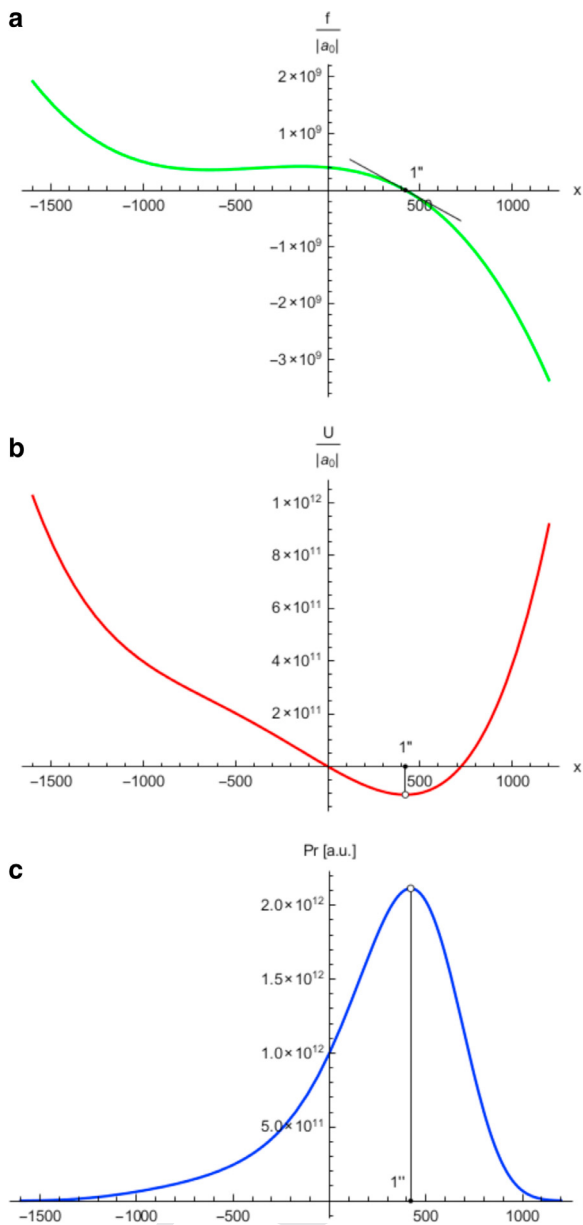


**Fig. 7.** Three complementary plots concerning the same region placed before the first tipping point of the backward-folded curve (or empirical data, for instance, for DAX) denoted in Fig. 6(b) by the character 'x'. The (mechanical) equilibrium point  $1'' (= x_{1''}^*) = 421.009$ , shown in the upper plot (a) as the single root of the equation  $f(x; P) = 0$ , is obtained directly from the empirical data (– the ordinate of this root shown in Fig. 6(b) is the time = 665 [td-11000]). The upper plot (a) shows the dependence of the force  $f(x; P)$ , (present in Eqs. (B.1) and (C.2)) vs.  $x$  for the values of (relative) coefficients  $a_1/a_0=1179.81$ ,  $a_2/a_0=278390$  and  $a_3/a_0=-4.00948 \times 10^8$  obtained in the C.4 ('Case before the bistable region') and common to all the plots (a), (b), and (c). In the middle plot (b) the corresponding potential,  $U(x; P)$ , is shown where the point  $1''$  is the sole stable equilibrium. In the bottom plot (c), the equilibrium probability distribution,  $Pr(x; P)$ , given by Eq. (B.5), is shown. Notably, variable  $x$  equals  $x^*$  only if  $x$  becomes a root of  $f$ . For interpretation of the references to colour in this figure legend, the reader is referred to the web version of this article.

**Fig. 8.** Three complementary plots concerning the same bifurcation (bistable) region (denoted by the arrow 'Before' in Fig. 6(b)) ahead of the catastrophic bifurcation threshold, denoted there by the vertical dashed straight line. The (mechanical) equilibrium points  $x_1^* = -626.473$ ,  $x_{1'}^* = -488.308$  and  $x_{1''}^* = 278.92$ , as roots of equation  $f(x; P) = 0$  (see Appendix C for details), are obtained directly from the empirical data (or backward-folded curve) shown there. The ordinates of these points (shown in Fig. 6(b)) are times = 669, 670, and 671 [td-11000], respectively. The upper plot (a) shows the dependence of the force,  $f(x; P)$ , (present in Eq. (B.1)) vs.  $x$  for the values of the relative coefficients  $a_1/a_0 = 835.861$ ,  $a_2/a_0 = -5022.94$  and  $a_3/a_0 = -8.53249 \times 10^7$  obtained in the C.2 ('Case of the bistable region') common to all the plots (a)–(c). In the middle plot (b) the corresponding bistable potential,  $U(x; P)$ , is shown. The points  $1$  and  $1''$  are stable equilibria, while  $1'$  is an unstable one (hence,  $\Delta x_{1,1''} = 905.393$ ). In the bottom plot (c) the bistable equilibrium probability distribution,  $Pr(x; P)$ , given by Eq. (B.5) is shown. The inset plots better visualize the behaviour of  $f$ ,  $U$  and  $Pr$  vs.  $x$  in a very restricted region containing the points  $1$  and  $1'$ . Notably, variable  $x$  equals  $x^*$  only if  $x$  becomes a root of  $f$ . For interpretation of the references to colour in this figure legend, the reader is referred to the web version of this article.

246 window where  $\lambda$  is an almost constant value),

$$ACF_{EST}(1) = \frac{1}{Var(x_t)} \frac{1}{T} \left[ \left( \sum_{t=1}^T x_t x_{t+1} \right) - \frac{1}{T} \left( \sum_{t=1}^T x_t \right) \left( \sum_{t=1}^T x_{t+1} \right) \right], \quad (1)$$

247 where  $T = 20$ . Using this estimator,  $-\lambda$  is calculated and presented in  
 248 in Fig. 5 by the red dots (without error bars), which almost ev-

249 erywhere fall within the error bars, thus their time dependence is  
 250 qualitatively similar, as expected. This result, together with the cor-  
 251 responding one for the coefficient  $AR(1)$  (shown by blue dots with  
 252 error bars in the same figure), is necessary to calculate equilibrium  
 253 states (stable and unstable) defined in the next paragraph by the  
 254 set of  $x^*$  values.

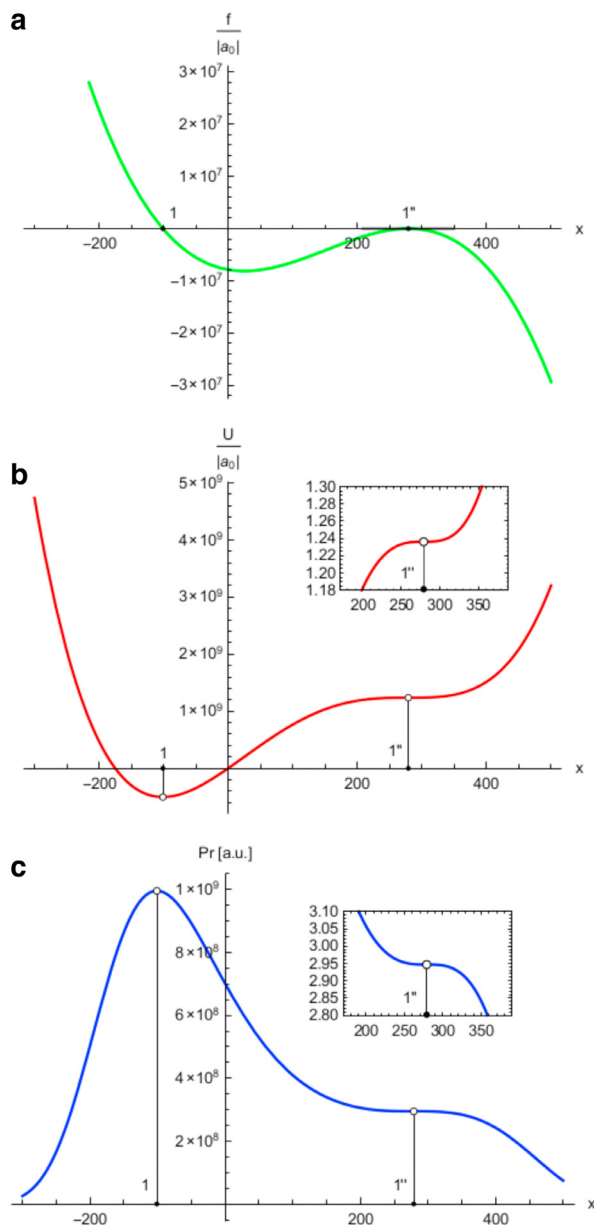


**Fig. 9.** Three complementary plots concerning the same bifurcation (bistable) region at the catastrophic bifurcation threshold; the region is denoted by the arrow 'At' in Fig. 6(b). All the curves are plotted for the same values of the relative coefficients  $a_1/a_0 = -456.67$ ,  $a_2/a_0 = 21359.70$  and  $a_3/a_0 = 7.87066 \times 10^6$  derived in C.1 ('Case of the catastrophic bifurcation transition') from the zeros of the  $f(x; P)$  curve. Apparently, the curve  $f/|a_0|$  vs.  $x$  in the upper plot (a) has a single twofold root  $x_1^* = x_{1''}^* = 278.92$  (– the ordinate of this root shown in Fig. 6(b) is the time = 675 [td-11000]). This root, being the second tipping point, is denoted in Fig. 6 by the character 'x' and placed in the immediate vicinity of the threshold. The first root  $x_1^* = -101.17$  is given directly by the empirical point placed on the threshold shown in Fig. 6(b) (hence,  $\Delta x_{1,1''} = 380.09$ ). In the middle plot (b) the corresponding bistable potential,  $U(x; P)$ , is shown (for the same relative coefficients as for the upper plot). The points 1 and 1'' are stable equilibria. In the bottom plot (c) the bistable equilibrium probability distribution,  $Pr(x; P)$ , given by Eq. (B.5), is shown. The inset plots better visualize the behaviour of  $f$ ,  $U$  and  $Pr$  vs.  $x$  in a very restricted region containing the point 1''. Notably, variable  $x$  equals  $x^*$  only if  $x$  becomes a root of  $f$ . For interpretation of the references to colour in this figure legend, the reader is referred to the web version of this article.

255 The empirical data shown in Fig. 5 provide the recovery rate,  
 256  $-\lambda$ , "smiles" with heights of minimums equal zero (to a good approx-  
 257 imation). Notably, the most significant result is that the minimum  
 258 of both curves is located at the same place, having (to good  
 259 approximation) the same height. Some small differences between  
 260 the two curves can (from this point of view) be neglected, particu-

larly as we can roughly expect that red dots have error bars of the  
 261 same order as blue dots. Indeed, the minimum of  $-\lambda$  is the source  
 262 of a slowing down effect (see Appendix B for details). This effect is  
 263 one of the necessary requirements (or signatures) for the existence  
 264 of a phase transition, in particular, of the catastrophic bifurcation  
 265 type.

Our approach is justified by assuming that  $\lambda$  is a piecewise, al-  
 267 most constant function of time, i.e., it is an almost fixed quantity  
 268 for the monthly set of empirical data points. We assume the same  
 269 for the shift coefficient  $b$  considered below. Hence,  $\lambda$  and  $b$  are  
 270 slowly varying functions of time (counted in months) in compar-  
 271 ison with the process  $x_t$  (counted in days). The difference in these  
 272 two time scales plays a basic role in our considerations.

#### 2.4. Empirical catastrophic bifurcation transitions

The shift coefficient  $b$  relates to the recovery rate  $-\lambda (> 0)$  and  
 275 fixed point (root)  $x^*$  through the key equality  $b = -\lambda x^*$  (see the  
 276 second Equation in (B.7)). Hence,  $x^*$  is plotted vs. time in Fig. 6  
 277 for three typical indices: (a) WIG, (b) DAX, and (c) DJIA. Apparently,  
 278 sufficiently far before the catastrophic bifurcation threshold (de-  
 279 noted by the vertical dashed straight lines in plots (a), (b), and (c))  
 280 and after it, the spontaneous reduction of error bars of the curve  
 281  $x^*$  vs. time ( $t$ ) is observed together with the smoothing out of  
 282 two substantially extended segments of this curve denoted by the  
 283 terms 'Before' and 'After', which can be identified as two evolving  
 284 separable equilibrium states of the system. The significant jumps of  
 285 empirical data points (leading to system instability) are seen solely  
 286 within the region between these two. The range of instability is  
 287 defined for plot (a) by points placed between time  $t = 557$  and  
 288  $t = 565$ , for plot (b) between time  $t = 670$  and  $t = 674$ , and for  
 289 plot (c) between time  $t = 471$  and  $t = 482$ . These empirical facts  
 290 are apparently of a rather universal nature, as they are consistently  
 291 observed on typical stock markets of small, mid and large capitali-  
 292 sations.

The structure of the unstable region enables us to outline the  
 294 backward folded curve – both its stable and unstable segments –  
 295 which exposes the so-called flickering phenomenon. Positions of  
 296 both tipping points (denoted by the character 'x') are defined solely  
 297 schematically (in crude approximation) to better indicate the fold-  
 298 ing effect. Although the location of the right tipping point is de-  
 299 fined with one-day precision, the location of the left tipping point  
 300 has about three days' uncertainty. The vertical uncertainty of both  
 301 tipping points can be assumed to be no greater than about 2000  
 302 to preserve the smooth character of the backward folded curve.  
 303 That is, all backward folded curves, which could be drawn to serve  
 304 as non-analytical eye guides, should be topologically equivalent.  
 305 Therefore, it is possible to construct the backward folded eye-guide  
 306 curves together with their tipping points as they are sufficiently  
 307 limited by the spatial constraints.

As indicated above, the precise location of the tipping points  
 309 is of no importance to us. What is important is solely the spec-  
 310 ific structure (shape) of the backward-folded curve, which prop-  
 311 els the dynamics over the unstable region. Indeed, the unstable  
 312 segment of this curve consists of a sequence of states responsible  
 313 for the flickering phenomena that is, for large oscillations across  
 314 these states – in the case of the absence of an unstable segment,  
 315 the flickering phenomena would be suppressed.

Flickering is well pronounced in Fig. 6, ahead of the negative  
 317 catastrophic spikes evident in plots (a), (b), and (c) and defining  
 318 the bistable regime. This flickering phenomenon appears within  
 319 the bistable region, where the sequence of unstable (intermedi-  
 320 ate) states or roots  $\{x_1^*\}$  (see Appendix B and Appendix C for de-  
 321 tails) placed on the hypothetical (dotted) curve causes the system  
 322 to bounce between these states and the sequence of stable states  
 323  $\{x_1^*\}$  indicated on the hypothetical lower (solid) curve. Indeed, this  
 324



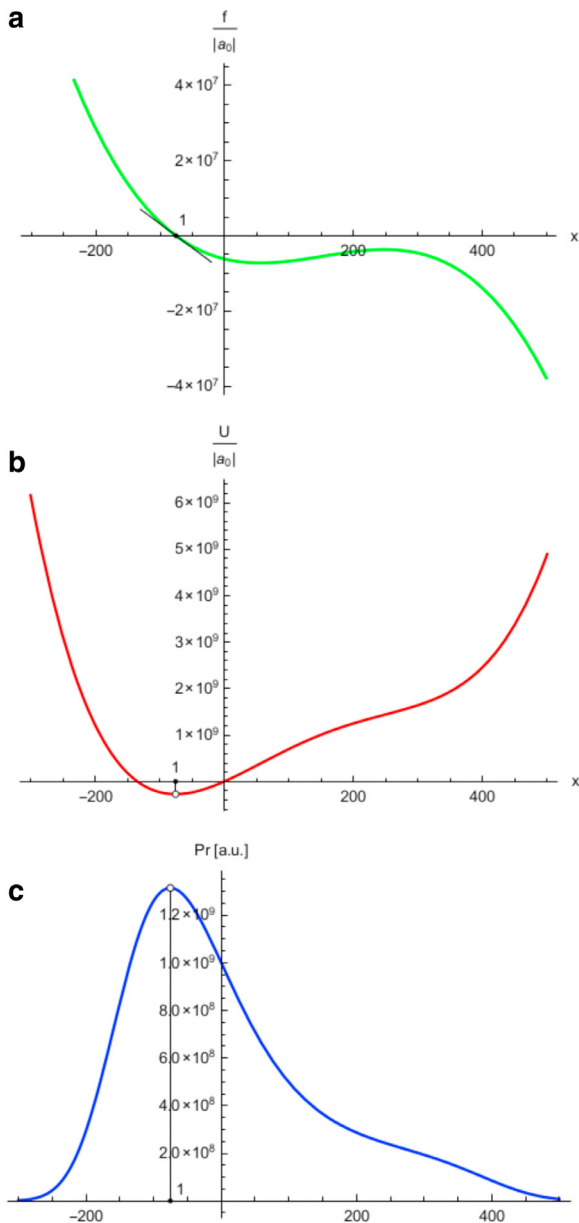


**Fig. 10.** Three complementary plots concerning the same region after the bifurcation (bistable) threshold (denoted by the vertical dashed straight line); the region was denoted in Fig. 6(b) by the arrow 'After'. All the curves were plotted for the same values of the relative coefficients  $a_1/a_0 = -456.67$ ,  $a_2/a_0 = 41709.50$  and  $a_3/a_0 = 6.1682 \times 10^6$  derived in C.3 ('Case after the catastrophic bifurcation transition') from the zeros of  $f(x; P)$  curve obtained from the empirical data shown in Fig. 6(b). The curve  $f/|a_0|$  vs.  $x$  in the upper plot (a) has a single root  $x_1^* = -75.39$  (– the ordinate of this root shown in Fig. 6(b) is the time = 680 [td-11000]). In the middle plot (b) the corresponding potential,  $U(x; P)$ , is shown. Point 1 is a stable equilibrium. In the bottom plot (c), the equilibrium probability distribution,  $Pr(x; P)$ , given by Eq. (B.5), is shown. Notably, variable  $x$  equals  $x^*$  only if  $x$  becomes a root of  $f$ . For interpretation of the references to colour in this figure legend, the reader is referred to the web version of this article.

325 bounce effect can cause, for instance, oscillations in the variance  
 326 ahead of the spikes shown in plots (a), (b), and (c) in Fig. 3. We  
 327 consider the existence of the flickering phenomenon and subse-  
 328 quent spike between two rather flat sequences of states as a pos-  
 329 sible result of a catastrophic bifurcation transition. This is dis-  
 330 cussed in detail in B.3 (see Eq. (B.13)). It should be emphasized  
 331 that the three-phase sequence observed: 'equilibrium–instability  
 332 (or flickering)–equilibrium' during the system evolution is essential

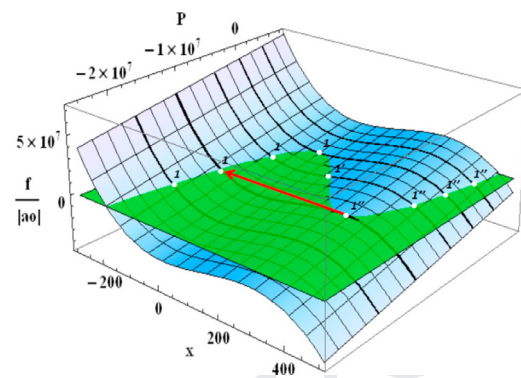


**Fig. 11.** A comprehensive three-dimensional schematic view showing the origin of the flat backward-folded curve  $x^*$  vs.  $P$  placed on a (semi-transparent) green plane. This backward-folded curve originated as a section of the green plane with the wavy blue surface. The points denoted by 1 and  $1''$  (white circles) are stable mechanical equilibria located, respectively, on the left and right segments of this curve. The points denoted by  $1'$  (also white circles) are unstable mechanical equilibria located on the backward-folded segment of this curve. The catastrophic bifurcation transition from the equilibrium state  $1''$  to 1 is indicated by the long red arrow. These particular points are placed on the catastrophic bifurcation curve (thicker than all other curves) located on the wavy blue surface. Note, that the singular behaviour of the schematic backward-folded curve in the vicinity of the catastrophic bifurcation threshold (cf. in plots (a), (b), (c) in Fig. 6) is absent here. The impact of the noise  $\eta_t$  on the states  $x_t$  and  $x_t^*$  is not visualized here. Notably, variable  $x$  becomes  $x^*$  only if  $x$  becomes a root of  $f$ . For interpretation of the references to colour in this figure legend, the reader is referred to the web version of this article.

333 for the formulation of a sound conjecture of the bistability or dy-  
 334 namic bifurcation.

335 The results shown in Fig. 6 constitute the basis for further dis-  
 336 cussion because they suggest that bifurcations or bistabilities on  
 337 financial markets can exist. Thus, they validate considering the tra-  
 338 jectory of  $x^*(t)$  as extrema (minima or maxima) of a hypotheti-  
 339 cal 'mechanical' potential curve (drawn in the third dimension, i.e.  
 340 along the third (vertical) additional axis which can be attached to  
 341 plots (a), (b), and (c) in Fig. 6).

342 **3. Mechanical-like view**

343 Following the article by [19] and by using basic results pre-  
 344 sented in Fig. 6, we provide a quantitative description founded on  
 345 the mechanical-like picture of a ball moving in the potential land-  
 346 scape. We consider snapshot pictorial views of different states of  
 347 the system on the pathway to regime change illustrated by a se-  
 348 quence of properly chosen Figs. 7–11. This pathway is defined by  
 349 dependence  $x^* = x^*(P)$ , where the driving (hidden) parameter  $P$  is,  
 350 by definition, a slowly-varying function of time (see Appendix C for  
 351 a detailed expression). The point  $x^*$  is a root of equation  $f(x; P) = 0$   
 352 – see the respective zeros 1,  $1'$  or/and  $1''$  shown (by small black  
 353 circles) in the upper plots (a) of the force  $f(x; P)$  vs.  $x$  in Figs. 7–10,  
 354 and also the sequence of points 1,  $1'$  and  $1''$  (white circles) present  
 355 in the summary of Fig. 11. In the middle plots (b) the potential  $U(x;$   
 356  $P)$  vs.  $x$  is shown, indicating that the points 1,  $1''$  are stable, while  
 357 point  $1'$  is unstable. Finally, in the bottom plots (c), the equilibrium  
 358 probability distribution,  $Pr(x; P)$  given by Eq. (B.5) is shown ver-  
 359 sus  $x$ . Figs. 8 and 9 show the most significant results of our work,  
 360 namely both a bifurcation (cf. Fig. 8) and a catastrophic bifurcation  
 361 (cf. Fig. 9) observed in empirical financial time series.

362 Let us examine the pathway to regime change with greater care.  
 363 When time increases, the system passes successive states defined  
 364 by the values of  $x^*$ , well pronounced in Fig. 6. The initial charac-  
 365 teristic state defined by a single value of  $x^*$  is shown in Fig. 7. It re-  
 366 presents the region ahead of the bifurcation. The central objective of  
 367 interest to us is defined in Fig. 8 by the three different values of  $x^*$ .  
 368 The borders of the bifurcation region, limited by tipping points, are

denoted in the plots in Fig. 6 by the character 'x'. The arrows show the possible transitions between the equilibrium points. The third, extremely interesting case of the catastrophic bifurcation transition is presented in Fig. 9. For this case, the points  $1'$  and  $1''$  coincide. The point  $x_{1''}^*$  is represented in Fig. 6 by the second character 'x'. In this case, the possible transition between the points  $1''$  and  $1$  is shown schematically by the arrow in Fig. 11. The last (fourth) case, illustrated by Fig. 10, is similar to the first one, as again it is defined by a single root, namely by 1.

Notably, the two segments of the folded backward curve  $x^*(P)$  containing the points 1 and  $1''$  (cf. Fig. 11) represent stable equilibria, while the third backward segment in between, containing the points of the  $1'$  type, represents an unstable equilibrium. If the system is driven slightly away from the stable equilibrium it will return to this state with the relaxation time  $\tau(P) = -1/\lambda(P)$  (cf. considerations in Appendix B in particular Eq. (B.9)). Otherwise, the system driven from the unstable equilibrium will move away (to one of the two stable equilibria). In fact, the backward segment of the curve  $x^*(P)$  (denoted by the dashed backward curves in the plots in Fig. 6) represents a border or a repelling threshold between the corresponding basins of attraction of the two alternative stable states (defined by the lower and the upper branches of the backward-folded curves, marked in the same figures by the solid curves).

In this work, we focus mainly on the analysis of stable equilibria. Two of them are the tipping points at which a tiny perturbation (spontaneous or systematic) can produce a sudden large transition (indicated, e.g. for the second tipping point, by a long arrow in Fig. 11). It should be noted that only in the vicinity of the stable equilibria, that is for the points placed on the lower or the upper branches of the folded curve, the variance of the detrended time series diverges according to a power-law (cf. Expression (B.11) in Appendix B). This is a direct consequence of the catastrophic slowing down (CSD), which can be well detected before the actual occurrence of the catastrophic transition. This divergence can be intuitively understood as follows. As the return time diverges, the impact of a shock does not decay (see solution Eq. (B.9)), and its accumulating effect increases the variance. Hence, CSD reduces the ability of the system to follow the fluctuations [53].

We explain in this Section how indicators (or early warnings) arise when the system approaches the regime shift or the catastrophic bifurcation transition (threshold). It is sufficient to consider the linear early warnings such as variance, recovery time, reddened power spectra and related quantities in the framework of the linearized theory defined by Eqs. (B.6) and (B.7). It is convenient to consider the nonlinear indicators (such as a non-vanishing skewness) by the approach based on the nonlinear and asymmetric part of the force  $f(x; P)$  (present in the first equality in (B.1)) and on its asymmetric potential  $U(x; P)$  (present in the second equality in (B.1)), both in the immediate vicinity of the regime shift – cf. plots in Fig. 9 concerning the case at the catastrophic bifurcation threshold.<sup>7</sup> This is one of the simplest viewpoints considered, for instance, in the article by Guttal and Jayaprakash [19].

#### 4. Concluding remarks

Following the supposition in [34] concerning the possibility of the existence of bifurcation transitions, in particular catastrophic ones, on financial markets, we have studied the principal and most significant indicators of such transitions on stock exchanges of small and mid to large capitalisations. Other indicators (not visualized in this work) relating to properties of noise also confirm this

supposition. All these indicators consistently show that the thresholds presented in Figs. 3, 5, 6, and 9 should be identified as signatures of a catastrophic bifurcation transition. It was a noteworthy surprise in our analysis that the catastrophic bifurcation threshold itself constitutes a consistent indicator in daily empirical data obtained from various stock exchanges. As we have observed, such a threshold – serving as an early indicator – is noticeable for several months before the global crash.

The basic results of this work consist of the well-established observations that: (i)  $\lambda$  is a negative quantity, and (ii) recovery rate  $-\lambda$  vanishes when the system approaches the catastrophic bifurcation threshold (cf. Fig. 5). This vanishing effect (together with the result mentioned below, concerning the shift parameter  $b$ ) permits us to formulate the hypothesis that the underlying phenomenon is a catastrophic (but not critical) slowing down. The significance of this result is furthermore underlined by the fact that  $\lambda$  is a fundamental quantity which (as we are able to prove) enters all other linear indicators and also participates in non-linear ones.

Apart from  $\lambda$ , we have also identified the shift parameter  $b$  (cf. Fig. 4 and, in particular, the insert figure presented there). Hence, we have been able to present an empirical trajectory consisting of fixed points  $x^*$  plotted vs. trading time  $t$ , and directly observe the catastrophic bifurcation transition preceded by the flickering phenomenon (cf. plots in Figs. 6). Furthermore, we have found that each catastrophic bifurcation transition is preceded by a singularity-like anti-peak, which appears to be a super-extreme event (see again the plots in Figs. 6). As a consequence, we have been able to construct a mechanical-like view of the bifurcation transitions, resulting in a bimodal shape of the (unconditional) equilibrium statistics<sup>8</sup> (see Figs. 8 and 9 for details).

Our contribution opens possibilities for numerous applications, for instance for forecasting, market risk analysis and financial market management. In addition, the approach stimulating our present work is derived in part from ecology [19,53,55,57], where sometimes an ecosystem undergoes a catastrophic regime shift (in the sense of the René Thom catastrophe theory [19] over a relatively short period of time. Hence, this opens the possibility for the methodological elements of our work to be applicable in such domains. Nevertheless, a word of warning is in place here, as one can easily deceive oneself by seeing deterministic dynamics at work in random data with a certain structure, as demonstrated for example in [36]. Criteria for validating the emergent nature of such structures can prevent this kind of over-interpretation, and devising such criteria constituted the main goal of this work.

#### Uncited references

Refs. [12,17,26,30,31,61,62].

#### Acknowledgments

We are grateful to Piotr Suffczyński for stimulating discussions. T.G., T.R.W., and R.K. acknowledge partial financial support from the Polish Grant No. 119 awarded in the First Competition of the Committee of Economic Institute, organized by the National Bank of Poland.

#### Appendix A. Detrending procedure

In order to model the long-term trend of the time series presented in Fig. 1, we used the following relaxation function of

<sup>7</sup> Notably, the upper plot indicates that the maximal value of discontinuity of the recovery rate  $-\lambda$  should exist at the bifurcation threshold. However, this value is too small to be recognized (as statistical errors are too large); cf. plots in Fig. 5.

<sup>8</sup> We can say that this observation is seen even better for WIG and DJIA than for DAX.

**Table A.1**

Values of fit parameters of the trend for WIG bull market ( $R^2 = 0.9986$ ).

Parameter	Value	Standard deviation
$t_c$	892 [td]	73 [td]
$\tau$	105 [td]	420 [td]
$\alpha$	0.57	0.23
$\omega$	0.0041 [td <sup>-1</sup> ]	0.0005 [td <sup>-1</sup> ]
$\Delta\omega$	0.0	0.0

**Table A.2**

Values of fit coefficients of the trend for WIG bull market ( $R^2 = 0.9986$ ).

Coefficient	Value [p]	Standard deviation [p]
$X_0 + X_1$	60081	85273
$X_1$	-8659	2352

**Table A.3**

Values of fit parameters of the trend for WIG bear market ( $R^2 = 0.9985$ ).

Parameter	Value	Standard deviation
$t_c$	810 [td]	0 [td]
$\tau$	272 [td]	20 [td]
$\alpha$	1.562	0.025
$\omega$	0.0431 [td <sup>-1</sup> ]	0.0005 [td <sup>-1</sup> ]
$\Delta\omega$	0.0065	0.0004

**Table A.4**

Values of fit coefficients of the trend for WIG bear market ( $R^2 = 0.9985$ ).

Coefficient	Value [p]	Standard deviation [p]
$X_0 + X_1$	41963	334
$X_1$	-2528	269

**Table A.5**

Values of fit parameters of the trend for DAX bull market ( $R^2 = 0.9985$ ).

Parameter	Value	Standard deviation
$t_c$	969 [td]	1 [td]
$\tau$	426 [td]	391 [td]
$\alpha$	0.52	0.03
$\omega$	0.00362 [td <sup>-1</sup> ]	0.00004; [td <sup>-1</sup> ]
$\Delta\omega$	0.0065	0.0004

**Table A.6**

Values of fit coefficients of the trend for DAX bull market ( $R^2 = 0.9985$ ).

Coefficient	Value [p]	Standard deviation [p]
$X_0 + X_1$	4698	82
$X_1$	-763	35

**Table A.7**

Values of fit parameters of the trend for DAX bear market ( $R^2 = 0.9977$ ).

Parameter	Value	Standard deviation
$t_c$	968 [td]	0 [td]
$\tau$	426 [td]	72 [td]
$\alpha$	1.12	0.03
$\omega$	0.0089 [td <sup>-1</sup> ]	0.0001; [td <sup>-1</sup> ]
$\Delta\omega$	0.0246	0.0001

**Table A.8**

Values of fit coefficients of the trend for DAX bear market ( $R^2 = 0.9977$ ).

Coefficient	Value [p]	Standard deviation [p]
$X_0 + X_1$	5464	70
$X_1$	-847	36

**Table A.9**

Values of fit parameters of the trend for DJIA bull market ( $R^2 = 0.9996$ ).

Parameter	Value	Standard deviation
$t_c$	627 [td]	3 [td]
$\tau$	333 [td]	38 [td]
$\alpha$	1.29	0.02
$\omega$	0.0107 [td <sup>-1</sup> ]	0.0002; [td <sup>-1</sup> ]
$\Delta\omega$	0.0220	0.0002

**Table A.10**

Values of fit coefficients of the trend for DJIA bull market ( $R^2 = 0.9996$ ).

Coefficient	Value [p]	Standard deviation [p]
$X_0 + X_1$	3486	40
$X_1$	-332	28

**Table A.11**

Values of fit parameters of the trend for DJIA bear market ( $R^2 = 0.9971$ ).

Parameter	Value	Standard deviation
$t_c$	640 [td]	0 [td]
$\tau$	165 [td]	191 [td]
$\alpha$	1.938	0.575
$\omega$	0.030 [td <sup>-1</sup> ]	0.070; [td <sup>-1</sup> ]
$\Delta\omega$	0.040	0.070

484 time  $t$ :

$$X(|t - t_c|) = (X_0 + X_1)E_\alpha\left(-\left(\frac{|t - t_c|}{\tau}\right)^\alpha\right) - X_1 \cos(\omega |t - t_c|) \cos(\Delta\omega |t - t_c|),$$

$$X_0, \alpha, \tau, t_c > 0, \tag{A.1}$$

485 separately valid both for the bullish and the bearish sides of a  
 486 given well-formed market bubble. (Predictions of Formula (A.1) are  
 487 shown in Fig. 1 using solid lines.) Here, we have  $\omega, \Delta\omega \ll 1$ , as  
 488 this is required in the theoretical derivation of the above equation;  
 489 see [28] for details. All the parameters with the corresponding fit-  
 490 ted values are listed in Tables A.1–A.12.

491 The Mittag-Leffler function  $E_\alpha(\dots)$  is defined as follows [40]:

$$E_\alpha\left(-\left(\frac{|t - t_c|}{\tau}\right)^\alpha\right) = \sum_{n=0}^{\infty} \frac{(-1)^n}{\Gamma(1 + \alpha n)} \left(\frac{|t - t_c|}{\tau}\right)^{\alpha n}. \tag{A.2}$$

492 Here  $t_c$  denotes the localization of the turning point where the  
 493 market changes its state from bullish to bearish,  $\tau$  plays the role  
 494 of the relaxation time of the order of one year, and  $\alpha$  is the shape

exponent. All the values of parameters and coefficients describing  
 495 this function for indexes of WIG, DAX, and DJIA bull markets and  
 496 bear markets are listed in the Tables. A.1–A.12. Notably, the coeffi-  
 497 cient of determination,  $R^2$ , is in no case smaller than  $R^2 = 0.9971$ .  
 498 The value of  $R^2$  close to 1 indicates that (A.1) is a properly selected  
 499 trend. However, such a selection does not exclude the possibility of  
 500 the existence of a deterministic drift component in the detrended  
 501 time series. We model the detrended time series entailing this  
 502 component together with the additive noise in Appendix B. This  
 503 is done using the first-order difference equation of the stochastic  
 504 dynamics (B.1), and in particular, locally in the vicinity of a fixed  
 505 point using Eq. (B.7).  
 506

**Table A.12**

Values of fit coefficients of the trend for DJIA bear market ( $R^2 = 0.9971$ ).

Parameter	Value [p]	Standard deviation [p]
$X_0 + X_1$	4010	110
$X_1$	−866	81

507 The trend function (A.1) consists of two different compo-  
 508 nents: (i) the main component based on the Mittag-Leffler func-  
 509 tion monotonically increasing for  $t \leq t_c$  and monotonically de-  
 510 creasing in the opposite case, and (ii) the higher-order oscillat-  
 511 ing component (the amplitude  $X_1$  of which is of the order of 10%  
 512 of the amplitude of the main component  $X_0 + X_1$ ). As required,  
 513 the trend function obtained in this way mainly exhibits the long-  
 514 term slowly-varying super-exponential growth, which precedes the  
 515 speculation-induced crash.

516 The trend we use is a function that we derived earlier as a rhe-  
 517 ological model of fractional dynamics of financial markets ([28]).  
 518 This model introduces the hypothesis that stock markets behave  
 519 like a viscoelastic biopolymer. That is, they are elastic (i.e., they  
 520 immediately respond) if the impact of an external force on a stock  
 521 market is sufficiently strong. But they are more like a liquid (plas-  
 522 tic) material in the case of a weak external force. That is, financial  
 523 markets behave analogically to a non-Newtonian liquid.

524 Among the fit parameters and coefficients for a given index (see  
 525 Tables. A.1–A.12), there always exists at least one (characterizing  
 526 the bull market or bear market) which is burdened by a large stan-  
 527 dard deviation. In this way the system is protected from arbitrage.

528 **Appendix B. Catastrophic slowing down**

529 In this Appendix, we consider linear indicators of the catas-  
 530 trophic slowing down or regime shift such as: (i) recovery rate and  
 531 time, (ii) variance, and (iii) reddened power spectra.

532 Let us suppose that detrended time-dependent time series  
 533  $x_t \stackrel{\text{def}}{=} X(t) - \text{Trend}(t)$ , where  $\text{Trend}(t)$  is the trend expressed by Eq.  
 534 (A.1), obeys the first-order difference equation of the stochastic dy-  
 535 namics

$$x_{t+1} - x_t = f(x_t; P) + \eta_t = -\frac{\partial U(x_t; P)}{\partial x_t} + \eta_t, \quad (\text{B.1})$$

536 where  $U$  plays the role of a mechanical potential, the additive  
 537 noise or stochastic force  $\eta_t$ ,  $t = 0, 1, 2, \dots$ , is a  $\delta$ -correlated<sup>9</sup> (0,  
 538  $\sigma^2$ ) random variable.  $P$  is a slowly varying driving (control, in gen-  
 539 eral a vector) parameter, the precise definition of which is given in  
 540 Appendix C.

541 In the spirit of the time dependent Ginzburg-Landau theory of  
 542 phase transition ([55]), we can assume that the potential  $U(x; P)$   
 543 is a polynomial of the fourth-order (hence, force  $f$  is a polynomial  
 544 of the third-order, cf. Appendix C). Now, our goal is to determine  
 545 coefficients of this polynomial from the properly detrended empiri-  
 546 cal data. For instance, in Figs. 7–10 plots of force  $f$ , in potential  $U$ ,  
 547 and equilibrium probability  $Pr$  vs. detrended time series (variable)  
 548  $x$  are already shown (using solid lines) for different values of pa-  
 549 rameter  $P$ . Furthermore, in the comprehensive Fig. 11, the plots of  
 550  $f$  are grouped into a three-dimensional visualisation.

551 Our goal is to utilize potential  $U(x; P)$  in the construction of an  
 552 unconditional equilibrium distribution,  $Pr(x; P)$ , of the detrended  
 553 time series and present how both quantities evolve across bistable

forms. This will provide a signature of a genuine (and not spurious) 554  
 or artificial) bifurcation transition. 555

B1. Equilibrium distribution of detrended time series 556

The differential formulation directly results from Eq. (B.1). Its 557  
 basic ingredient is the Langevin dynamics [55,60], taking the form 558  
 of the massless stochastic dynamic equation 559

$$\frac{\partial x_t}{\partial t} = -\frac{\partial U(x_t; P)}{\partial x_t} + \eta_t. \quad (\text{B.2})$$

This equation is equivalent to the quasilinear (according to van 560  
 Kampen’s terminology, [60]) Fokker-Planck equation 561

$$\frac{\partial Pr(x, t; P)}{\partial t} = -\frac{\partial j(x, t; P)}{\partial x}, \quad (\text{B.3})$$

562 which is a form of the continuity equation (a conservation law) for  
 563 the probability density of the current, i.e. the detrended time series  
 564  $Pr(x, t; P)$ , where the current density is given by the constitutive  
 565 equation

$$j(x, t; P) = f(x; P) Pr(x, t; P) - \frac{\sigma^2}{2} \frac{\partial Pr(x, t; P)}{\partial x}. \quad (\text{B.4})$$

566 The equilibrium (time-independent) solution of Eq. (B.3) (ob-  
 567 tained directly from the requirement that no current is present in  
 568 the system, (i.e. by assuming that  $j(x, t) = 0$  in Eq. (B.4)) is given  
 569 by

$$Pr(x; P) \sim \frac{2}{\sigma^2} \exp\left(-\frac{2}{\sigma^2} U(x; P)\right), \quad (\text{B.5})$$

570 where potential  $U(x; P)$  already appeared in Eqs. (B.1) and (B.2).

571 The long-term, slowly-varying evolution of the above given dis-  
 572 tribution shown in Figs. 7–10 as  $U(x; P)$  versus  $P$  was found from  
 573 empirical data (see Appendix C for details). Indeed, the uncondi-  
 574 tional equilibrium distribution (B.5) exhibits the expected bistable  
 575 shape slightly before (see Fig. 8) and at the catastrophic bifurcation  
 576 transition, that is within the bifurcation region (see Fig. 9).

B2. Analysis of the linear stability 577

578 In this section, we study the linear stability of the equilibrium,  
 579 that is we consider the relaxation of the system which was slightly  
 580 knocked out of equilibrium [63]. The equilibrium of the system is  
 581 defined by the roots (or fixed points) of the function  $f(x; P)$ . In  
 582 Sec. 3, we argue that these roots can be viewed as the mechanical-  
 583 like equilibria. 583

584 The linear expansion of  $f(x; P)$  at the fixed point  $x^*$ , gives

$$y_{t+1} - y_t = f(x^*(P); P) + \lambda y_t + \eta_t = \lambda y_t + \eta_t \quad (\text{B.6})$$

$$\Leftrightarrow y_{t+1} = AR(1)y_t + \eta_t$$

585 as, by the definition of a root,  $f(x^*(P); P)$  vanishes. We will  
 586 use the following notation: (i) for the displacement from an  
 587 equilibrium<sup>10</sup> or the (non-normalized) order parameter  $y_t = x_t -$   
 588  $x^*(P)$ ,  $t = 0, 1, 2, \dots$  and (ii) for rate  $\lambda(x^*(P); P) = \frac{\partial f(x; P)}{\partial x} \Big|_{x=x^*(P)}$ .  
 589 The autoregressive coefficient of the first-order  $AR(1) = 1 + \lambda$ .

590 The formula in the second line of Eq. B.6, rewritten in the  
 591 form

$$x_{t+1} = (1 + \lambda)x_t + b + \eta_t, \quad b = A(0) = -\lambda x^*, \quad (\text{B.7})$$

<sup>9</sup> Here,  $\delta$  is the Kronecker delta, while  $t$  indexes trading days within a given trad-  
 ing month (consisting of twenty-one trading days). The trading month is our time  
 window, where  $\lambda$  is approximately constant.

<sup>10</sup> The set of variables  $y_t$ ,  $t = 0, 1, 2, \dots$  is also called the first-order autoregres-  
 sive time series.

593 makes it possible to obtain the recovery rate  $-\lambda (> 0)$  and fixed  
 594 point  $x^*$  vs. trading days from the fits to empirical data represented  
 595 by successive sample regression plots, such as shown, for instance,  
 596 in Fig. 4.

597 Each plot in this figure consists of 20 points of daily observa-  
 598 tions (i.e. covering a single month) at the closing, which appears to  
 599 be the optimal number for observing the slowing down to zero of  
 600 the recovery rates shown in the plots in Fig. 5<sup>11</sup> with a satisfactory  
 601 resolution. The error bar of each individual point placed in these  
 602 plots comes from the above-mentioned fits as a standard deviation  
 603 of the straight line slope. (The corresponding points without er-  
 604 ror bars were found independently from Expression (1)). Obviously,  
 605 these fits also give the straight line shift  $b$  vs. trading days. The  
 606 resulting combined quantity  $-b/\lambda$  is presented in plots in Fig. 6  
 607 vs. trading days. We obtain a surprisingly small statistical error for  
 608 these fits. However, we tacitly assumed that coefficients  $\lambda$  and  $b$   
 609 were slowly-varying functions of trading days. These fits constitute  
 610 the empirical basis for our further considerations.

611 The solution of Eq. (B.6) is

$$y_t = (1 + \lambda)^t y_0 + (1 + \lambda)^{t-1} \sum_{\tau=0}^{t-1} \eta_\tau (1 + \lambda)^{-\tau} \approx \exp(\lambda t) \left[ y_0 + \int_0^t \eta_\tau \exp(-\lambda \tau) d\tau \right] \quad (B.8)$$

612 and (as  $\langle \eta_\tau \rangle = 0$ ) its average

$$\langle y_t \rangle = (1 + \lambda)^t y_0 \approx \exp(\lambda t) y_0, \quad (B.9)$$

613 where the first equality in (B.8) is valid for  $t \geq 1$  (for  $t = 0$  the so-  
 614 lution  $y_{t=0} = y_0$ ). The second approximate equality in (B.8) is valid  
 615 solely for the case of  $|\lambda| \ll 1$  and  $t \gg 1$ , that is for the immediate  
 616 vicinity of the threshold (shown in Figs. 2, 3, and 5 by the vertical  
 617 dashed straight lines) and for a sufficiently long time.

618 From Eq. (B.9), it follows that a given equilibrium state is stable  
 619 (i.e.,  $\langle y_{t \rightarrow \infty} \rangle \rightarrow 0$  for  $y_0 \neq 0$  and  $\langle y_t \rangle = 0$  for  $y_0 = 0$ ) if and only  
 620 if<sup>12</sup>  $|1 + \lambda| < 1 \Leftrightarrow -2 < \lambda < 0$ ; otherwise it is unstable. Hence, the  
 621 local minima of the potential curve (e.g., points 1 and 1'' in the  
 622 bottom plot in Fig. 8) define stable equilibria, while the local max-  
 623 imum of the potential curve (e.g., point 1' again in the bottom plot  
 624 in Fig. 8) define the unstable equilibrium. The most relevant states  
 625 of the system are stable equilibrium points  $x_1^*$  and  $x_{1''}^*$ , shown in  
 626 Fig. 9 and in Fig. 11 (where they are connected by the arrow), as  
 627 they define the border of the bifurcation region. Hence, they are  
 628 referred to as the catastrophic bifurcation points or tipping points.  
 629 The quantity  $\tau \stackrel{\text{def.}}{=} -1/\lambda$  can be interpreted as the relaxation (re-  
 630 covery or return) time solely for the stable (mechanical) equilibria.  
 631 This is the characteristic time for the system to return to the equi-  
 632 librium state after being knocked out of it.

633 **B3. Generic properties of the first-order autoregressive time series**

634 It is well-known [7,16] that particularly useful quantities, i.e.  
 635 variance, covariance and autocorrelation function, as well as the  
 636 power spectrum, are related. We calculate them by exploiting an  
 637 exact solution given by the first equality in (B.8).

638 Firstly, we calculate the covariance,

$$\begin{aligned} \text{Cov}(y_t y_{t+h}) &= \langle y_t y_{t+h} \rangle - \langle y_t \rangle \langle y_{t+h} \rangle = (1 + \lambda)^{|h|} \text{Var}(y_t) = \\ \text{Cov}(x_t x_{t+h}) &= (1 + \lambda)^{|h|} \text{Var}(x_t) \end{aligned}$$

<sup>11</sup> This figure is the result of the linear transformation  $(1 + \lambda \rightarrow -\lambda)$  of Fig. 5. The empirical data points in Fig. 5 are credible, as they come from two independent sources, providing mutually consistent results.

<sup>12</sup> We observed that for our empirical data a more restrictive inequality  $-1 < \lambda < 0$  is obeyed.

$$\begin{aligned} \Leftrightarrow \text{ACF}(h) &= \frac{\text{Cov}(y_t y_{t+h})}{\text{Var}(y_t)} = \frac{\text{Cov}(x_t x_{t+h})}{\text{Var}(x_t)} = (1 + \lambda)^{|h|} \\ \Rightarrow \text{ACF}(h) &\approx \exp(\lambda |h|), \quad h = 0, \pm 1, \pm 2, \dots, \quad (B.10) \end{aligned}$$

639 where variance  $\text{Var}(y_t)$  is given (after straightforward calculations)  
 640 by the formula

$$\begin{aligned} \text{Var}(y_t) &= \langle y_t^2 \rangle - \langle y_t \rangle^2 = \text{Var}(x_t) \\ &= \text{Var}(y_0)(1 + \lambda)^{2t} - \frac{1}{\lambda(2 + \lambda)} [1 - (1 + \lambda)^{2t}] \sigma^2, \quad (B.11) \end{aligned}$$

641 where the notation  $\langle \dots \rangle$  denotes an average over the noise and the  
 642 initial conditions (within the statistical ensemble of solutions  $y_t$   
 643 given by Eq. (B.8)). The resultant equality in (B.10) is obeyed for  $|\lambda|$   
 644  $\ll 1$ . Furthermore, at a short-time limit, i.e., for  $2t \ll N^{-1}$ ,  $\text{Var}(y_t)$   
 645 simplifies into the form

$$\text{Var}(y_t) \approx \text{Var}(y_0)(1 + 2\lambda t) + t\sigma^2 \approx \text{Var}(y_0) + \sigma^2 t. \quad (B.12)$$

646 For the asymptotic time limit, i.e., for  $t \rightarrow \infty$ , Eq. (B.11) reduces  
 647 (for fixed  $\lambda$ ) to the form

$$\text{Var}(y_t) \approx -\frac{\sigma^2}{\lambda(2 + \lambda)}, \quad (B.13)$$

648 which diverges for vanishing  $\lambda$ . We hypothesise that by taking into  
 649 account the flickering phenomenon we will obtain a significant in-  
 650 crease in the variance within the bifurcation region. In general,  
 651 the analytical calculation of variance requires the solution of the  
 652 nonlinear Eq. (B.1) for  $f$ , given, in our case, by the polynomial (de-  
 653 fined further in the text by Eq. (C.2)), which remains an unsolved  
 654 challenge.

655 The coefficient  $1 + \lambda$  (present, for instance, in (B.10)) is the lag-  
 656 1 autocorrelation function, which can be found directly from the  
 657 empirical data (cf. Fig. 5). Apparently, it does not depend on the  
 658 variance.

659 It can be easily proven by using Solution (B.8) that any odd mo-  
 660 ment of the variable  $y_t$  asymptotically vanishes. Hence, from Eq.  
 661 (B.11), we find that within the linear theory, the skewness also  
 662 vanishes.

663 Furthermore, it can be easily verified (by using Solution (B.8))  
 664 that the excess kurtosis vanishes if variables  $y_0$  and  $\eta_t$  are drawn  
 665 from some Gaussian distributions. That is, within the scope of the  
 666 linear theory (i.e. in the vicinity of the threshold) the distribu-  
 667 tion of variable  $y_t$  can be Gaussian, of variance given by Expression  
 668 (B.11) and centred around the mean value  $\langle y_t \rangle = y_0(1 + \lambda)^t$ .

669 **Appendix C. Approximation of force  $f$  by the third-order polynomial**

670 Let us assume that the potential  $U$ , used in Eq. (B.1), is defined  
 671 by the fourth-order polynomial

$$U(x; P) = A_0 x^4 + A_1 x^3 + A_2 x^2 + A_3 x + A_4, \quad (C.1)$$

672 where  $A_l, l = 0, 1, \dots, 4$ , are its real coefficients related to the  
 673 (combined) parameter  $P$  – this relation is considered further in this  
 674 Section. Moreover, we can assume that the coefficient  $A_0 > 0$ . This  
 675 is dictated by the empirical data shown in Fig. 6, where the se-  
 676 quence of states (roots)  $x_{1''}^*$  and  $x_1^*$  placed respectively on the up-  
 677 per and lower segments of the backward folded curves are con-  
 678 sidered as the stable (mechanical) equilibrium states. Both these  
 679 roots have opposite signs, which results in the corresponding signs  
 680 of the coefficients.

681 According to the definition of potential (see Eq. (B.1)), force  $f$  is  
 682 a polynomial of one order of magnitude lower

$$f(x; P) = a_0 x^3 + a_1 x^2 + a_2 x + a_3, \quad (C.2)$$

683 here coefficients  $a_{4-l} = -lA_{4-l}, l = 1, \dots, 4$ , where  $a_0 < 0$ .

685 Below, we consider following characteristic cases: (a) the catastro-  
686 phic bifurcation transition at catastrophic bifurcation threshold  
687 (regarding Fig. 9), (b) the transition before the catastrophic bifurca-  
688 tion transition (but within bistable region regarding Fig. 8), (c) the  
689 transition present after it (regarding Fig. 10), and (d) the analog-  
690 ous transition present before the bistable region (regarding Fig. 7).

691 The aim of this Section is to express the coefficients of the poly-  
692 nomial (C.2) in terms of the roots of this polynomial. These roots  
693 can be easily extracted from empirical data shown in Fig. 6. Us-  
694 ing these coefficients, we are able to plot the force and potential  
695 curves (see Figs. 7–10 for details) and give a mechanical interpre-  
696 tation to the catastrophic bifurcation transition.

697 *C1. Case of the catastrophic bifurcation transition*

698 Let us focus on the case (a) (presented in Fig. 9) concerning  
699 the catastrophic bifurcation transition. This means that the coeffi-  
700 cients  $a_l, l = 0, \dots, 3$ , should provide a corresponding parameteri-  
701 sation, which results in a curve  $f(x; P)$  vs.  $x$  in the form shown in  
702 Fig. 9. (We relate these coefficients to the parameter  $P$  at the end  
703 of this Section.)

704 Now, we can provide the detailed goals of this case. They are as  
705 follows:

- 706 (i) derivation of the root  $x_1^*$  and twofold root  $x_{1''}^*$  of the polynomial  
707 (C.2) and hence calculation, for instance, of the catastrophic bi-  
708 furcation jump,  $\Delta x_{1,1''}^* = x_{1''}^* - x_1^*$ , as a function of polynomial  
709 coefficients,
- 710 (ii) the solution of the inverse problem, that is derivation of the  
711 relative parameters  $a_1/a_0, a_2/a_0$ , and  $a_3/a_0$  by means of roots  $x_1^*$   
712 and  $x_{1''}^*$ , which can be obtained from the empirical data shown  
713 in Fig. 6.

714 Notably, the catastrophic bifurcation transition  $1'' \Rightarrow 1$  (cf. the  
715 upper plot in Fig. 9 and the transition denoted by the arrow in  
716 Fig. 11) beginning at the point  $1''$  – which is not only the largest  
717 (twofold) root of polynomial  $f$  but it also provides the position of  
718 its local maximum; hence, it is an inflection point of the curve  $U$   
719 vs.  $x$  (cf. upper and middle plots in Fig. 9). Considering the canon-  
720 ical representation

$$\frac{1}{a_0} f(x; P) = (x - x_1^*)(x - x_{1''}^*)^2, \tag{C.3}$$

721 and utilizing Eq. (C.2), we obtain

$$\begin{aligned} \frac{\partial f(x; P)}{\partial x} \Big|_{x=x_0, x_{1''}^*} = 0 &\Leftrightarrow 3x_{0,1''}^{*2} + 2\frac{a_1}{a_0}x_{0,1''}^* + \frac{a_2}{a_0} = 0, \\ &\Leftrightarrow x_1^* = \frac{1}{2}(3x_0^* - x_{1''}^*), \end{aligned} \tag{C.4}$$

722 where  $x_0^*$  is the first inflection point of the curve  $U$  vs.  $x$  (see the  
723 middle plot in Fig. 9) and it is the local minimum of the curve  $f$  vs.  
724  $x$  (see the upper plot in Fig. 9). However, this point is not explicitly  
725 shown there.

726 From Eqs. (C.4) and Eq. (C.3), we obtain

$$\begin{aligned} x_{0,1''}^* &= x_{ip}^f \mp \frac{1}{3}\sqrt{D}, \quad D \stackrel{\text{def}}{=} \left(\frac{a_1}{a_0}\right)^2 - 3\frac{a_2}{a_0}, \\ x_1^* &= x_{ip}^f - \frac{2}{3}\sqrt{D}, \end{aligned} \tag{C.5}$$

727 where for the first upper equation sign – represents the location of  
728 the minimum  $x_0^*$ , the sign + represents the location of the root  $x_{1''}^*$ ,  
729 and we assumed  $D > 0$  as both real roots of Eq. (C.4) should exist.  
730 Besides, we can easily derive (from the vanishing of the second  
731 derivative  $f$  over  $x$ ) that  $x_{ip}^f$ , present in (C.5), is the inflection point  
732 of  $f$  (cf. the upper plot in Fig. 9),

$$\frac{\partial^2 f(x; P)}{\partial x^2} \Big|_{x=x_{ip}^f} = 0 \Leftrightarrow x_{ip}^f = -\frac{1}{3}\frac{a_1}{a_0}. \tag{C.6}$$

733 As follows from Eq. (C.5), both extrema  $x_0^*$  and  $x_{1''}^*$  are located sym-  
734 metrically on either sides of the inflection point  $x_{ip}^f$ . That is the  
735 position  $x_0^*$  of the minimum is located on the left-hand side, while  
736 the position of the root  $x_{1''}^*$  is on the right-hand side, both being  
737 at the same distance from the position of the inflection point.

738 From Eqs. (C.5), we obtain the catastrophic bifurcation jump in  
739 the form of

$$\Delta x_{1,1''}^* = \sqrt{D} = \frac{1}{2a_0} \frac{\partial^2 f(x; P)}{\partial x^2} \Big|_{x=x_{1''}^*}, \tag{C.7}$$

740 which can be easily determined from the curves plotted in Fig. 9.  
741 Moreover, the latter equality means that taking into account the  
742 quadratic term in the expansion of (B.1) vs.  $x_t$  could be a promis-  
743 ing approach. A step, based on empirical data, beyond the linear  
744 approximation utilized in the derivation of Eq. (B.6), could provide  
745 more detailed information, e.g., concerning autocorrelation in the  
746 vicinity of the catastrophic bifurcation transition.

747 From Eqs. (C.5) and (C.6), we derive the solution of the inverse  
748 problem in the form,

$$\begin{aligned} \frac{a_1}{a_0} &= -(2x_{1''}^* + x_1^*) \leq 0, \\ \frac{a_2}{a_0} &= x_{1''}^*(x_{1''}^* + 2x_1^*) \geq 0, \end{aligned} \tag{C.8}$$

749 together with the constraint for the relative free parameter

$$\frac{a_3}{a_0} = -x_1^*(x_{1''}^*)^2 \geq 0. \tag{C.9}$$

750 The latter relation makes the above procedure self-consistent.

751 By identifying the roots  $x_1^* = -101.17$  and  $x_{1''}^* = 278.92$  from the  
752 empirical data shown in Fig. 6(b) as the right tipping point and the  
753 one placed on the bifurcation threshold, respectively, we derive the  
754 relative parameters in question  $a_1/a_0 = -456.67, a_2/a_0 = 21359.70$   
755 and  $a_3/a_0 = 7.87066 \times 10^6$ . Thus, we obtained the unique values  
756 of parameters without any fitting routine, i.e. the parameters are  
757 not the fitting ones. In addition, the three inequalities given above  
758 lead to the following ones:  $a_1 \geq 0, a_2 \leq 0, a_3 \leq 0$ . The bottom plots  
759 shown in Figs. 8–11 tacitly assume that the parameter  $P$  monoton-  
760 ically depends on time (counted on a monthly time scale) at least  
761 in the vicinity of the CBT. The vector parameter  $P$  consists, in our  
762 case, of only two independent components, e.g.,  $x_1^*$  and  $x_{1''}^*$ . This is  
763 sufficient to perform stochastic simulation at the catastrophic tran-  
764 sition point.

765 *C2. Case of the bistable region*

766 The case considered here (i.e., the case represented by Fig. 8) is  
767 a generalisation of the one discussed in the subsection above. That  
768 is, we consider a variable  $x$  placed inside the bifurcation region,  
769 where three different real roots exist (cf. backward-folded curves  
770 shown in Fig. 6 and schematically shown in Fig. 11).

771 The goal of this subsection is analogous to that considered  
772 above, i.e., to extract coefficients of the polynomial (C.2) by using  
773 its roots found from the empirical data (shown in the above men-  
774 tioned figures). By assuming that the polynomial (C.2) has three  
775 real different roots and by comparing Eq. (C.2) with its multiplica-  
776 tive form  $\frac{1}{a_0} f(x; P) = (x - x_1^*)(x - x_1^*)(x - x_{1''}^*)$ , we obtain the re-  
777 lations sought for the coefficients of the polynomial

$$\begin{aligned} \frac{a_1}{a_0} &= -(x_{1''}^* + x_1^* + x_1^*), \\ \frac{a_2}{a_0} &= x_1^*x_{1''}^* + x_1^*x_1^* + x_1^*x_1^*, \\ \frac{a_3}{a_0} &= -x_1^*x_1^*x_{1''}^*. \end{aligned} \tag{C.10}$$

778 The equations above are a generalization of the corresponding Eqs.  
779 (C.8) and (C.9), as we obtain these by inserting  $x_{1''}^* = x_{1''}^*$  in Eqs.  
780 (C.10).

Fig. 8 was constructed by using coefficients obtained from Eqs. (C.10) by introducing into their right-hand sides, the following empirical values of the roots:  $x_1^* = -626.473$ ,  $x_1^{**} = -488.308$ ,  $x_1^{***} = 278.92$ , taken, for instance, from the backward-folded curve shown in Fig. 6(b). From (C.10), we obtain the unique values of the relative parameters:  $a_1/a_0 = 835.861$ ,  $a_2/a_0 = -5022.94$ ,  $a_3/a_0 = -8.53249 \times 10^8$ . Apparently, this situation is analogous to the previous one (considered the above).

### C3. Case after the catastrophic bifurcation transition

For this case (represented by Fig. 10), we have an insufficient amount of empirical data for a unique solution, as only a single real root  $x_1^*$  can be identified (roots  $x_1^{**}$  and  $x_1^{***}$  are the complex conjugates). Hence, we deal only with a single relation between the coefficients of the polynomial

$$\frac{1}{a_0} f(x_1^*; P) = -(x_1^*)^3 - \frac{a_1}{a_0} (x_1^*)^2 - x_1^* \frac{a_2}{a_0} - \frac{a_3}{a_0} = 0, \quad (\text{C.11})$$

which makes the ratio of the parameters  $a_3/a_0$  dependent on  $x_1^*$ ,  $a_1/a_0$ , and  $a_2/a_0$ . Therefore, the driving vector parameter can be defined as  $P = (x_1^*, a_1/a_0, a_2/a_0)$ , where relative parameters  $a_1/a_0$  and  $a_2/a_0$  are free. For instance, in Fig. 10 we show plots for the root  $x_1^* = -75.3875$ , as well as the ratios of the parameters  $a_1/a_0 = -456.67$ ,  $a_2/a_0 = 41709.50$ , and  $a_3/a_0 = 6.1682 \times 10^6$ .

### C4. Case before the bistable region

We deal with an analogous situation as given above if  $x$  is placed before the catastrophic bifurcation region and (simultaneously) outside of the bistable region. Then, we are again dealing with a single real root, e.g.,  $x_1^{**} = 421.009$ , while the roots  $x_1$  and  $x_1^*$  are complex conjugates. For instance, in Fig. 7 we show plots for the ratios of the parameters  $a_1/a_0 = 1179.81$ ,  $a_2/a_0 = 278390$  and  $a_3/a_0 = -4.00948 \times 10^8$ .

Fortunately, the cases represented by Figs. 7 and 10, and defined by two free relative parameters  $a_1/a_0$  and  $a_2/a_0$ , are not particularly interesting because the regions concerned are outside the most interesting bistable regime.

## References

[1] Albert R, Barabási A-L. Statistical mechanics of complex networks. Rev Mod Phys 2001;74:47–97.  
 [2] . In: Albeverio S, Jentsch V, Kantz H, editors. Extreme events in nature and society. Berlin: Springer-Verlag; 2006.  
 [3] Badii R, Politi A. Complexity. Hierarchical structures and scaling in physics. Cambridge: Cambridge Univ. Press; 1997.  
 [4] Barunik J, Vosvrda M. Can a stochastic cusp catastrophe model explain stock market crashes? J Econ Dyn Control 2009;33:1824–36.  
 [5] Belej M, Kulesza S. Real estate market under catastrophic change. Acta Phys Pol 2013;123:497–501.  
 [6] Brock WA, Carpenter SR, Scheffer M. Regime shifts, environmental signals, uncertainty and policy choice. In: Norberg J, Cumming G, editors. A theoretical framework for analyzing social-ecological systems. New York: Columbia Univ. Press; 2006. p. 180–206.  
 [7] Brockwell PJ, Davis RA. Time series: theory and methods. Berlin: Springer-Verlag; 1991.  
 [8] Carpenter SR, Brock WA. Rising variance: a leading indicator of ecological transitions. Ecol Lett 2006;9:308–15.  
 [9] Carpenter SR, Brock WA, Cole JJ, Kitchell JF, Pace ML. Leading indicators of trophic cascades. Ecol Lett 2008;11:128–38.  
 [10] Chang G, Feigenbaum J. A bayesian analysis of log-periodic precursors to financial crashes. Quant Finance 2006;6:15–36.  
 [11] Dorogovtsev SN, Goltsev AV, Mendes JFF. Critical phenomena in complex networks. Rev Mod Phys 2008;80:1275–335.  
 [12] Erdélyi A. Tables on integral transforms. I. In: Based in part, on notes left by H. Bateman and compiled by the staff of the Bateman manuscript project. New York: McGraw-Hill Book Comp. Inc.; 1954.  
 [13] Fantazzini D, Geraskin P. Everything you always wanted to know about log-periodic power laws for bubble modelling but were afraid to ask. Eur J Finance 2013;19:366–91.  
 [14] Filimonov V, Sornette D. Spurious trend switching phenomena in financial markets. Eur Phys J B 2012;85(15/1–5).

[15] Fry JM. Exogenous and endogenous market crashes as phase transitions in complex financial systems. EPJ B 85 2012;405.  
 [16] Fuller WA. Introduction to statistical time series. Canada: J. Wiley & Sons, Inc.; 1976.  
 [17] Geweke J, Porter-Hudak S. The estimation and application of long-memory time series models. J Time Ser Anal 1983;4:221–37.  
 [18] Gottinger H-W. Complexity and catastrophe, applications of dynamic system theory. In: Kyn O, Schrettl W, editors. On the stability of contemporary economic systems: proceedings of the third Reisenburg Symposium. Vandenhoeck & Ruprecht; 1979. p. 422–38.  
 [19] Guttal V, Jayaprakash C. Changing skewness: an early warning signal of regime shifts in ecosystems. Ecol Lett 2008;11:450–60.  
 [20] Haldane AG, May RM. Systemic risk in banking ecosystems. Nature 2011;469:351–5.  
 [21] Hohenberg P, Halperin B. Theory of dynamic critical phenomena. Rev Mod Phys 1977;59:435–79.  
 [22] Jakimowicz A. Catastrophes and chaos in business cycle theory. Acta Phys Pol A 2010;117:640–6.  
 [23] Jiang SM, Cai SM, Shou T, Zhou PL. Note on two-phase phenomena in financial markets. Chin Phys Lett 2008;25(6):2319–22.  
 [24] Johnson N. Proposing policy by analogy is risky. Nature 2011;469:302–302.  
 [25] Johnson NF, Hui PJ. Financial market complexity. Oxford: Oxford Univ. Press; 2007.  
 [26] Kantz H, Schreiber T. Nonlinear time series analysis. Cambridge: Cambridge, Univ. Press; 2000.  
 [27] Paul W, Baschnagel J. Stochastic processes. From physics to finance. Berlin: Springer-Verlag; 1999.  
 [28] Kozłowska M, Kasprzak A, Kutner R. Fractional market model and its verification on the Warsaw stock exchange. Int J Mod Phys C 2008;19:453–69.  
 [29] Kozłowska M, Kutner R. Singular dynamics of various macroeconomic sectors. Acta Phys Pol 2010;117:630–6.  
 [30] Kubo R, Toda M, Hashitsugu N. Statistical physics II. Nonequilibrium statistical mechanics. Berlin: Springer-Verlag; 1985.  
 [31] Kutner R. Hierarchical spatio-temporal coupling in fractional wanderings. (i) continuous-time weierstrass flights. Physica A 1999;264:84–106.  
 [32] Kutner R, Binder K, Kehr KW. Diffusion in concentrated lattice gases. v. particles with repulsive nearest-neighbor interaction on the face-centered-cubic lattice. Phys Rev B 1983;28:1846–58.  
 [33] Landau DP, Binder K. A guide to Monte Carlo simulations in statistical physics. Cambridge: Cambridge Univ. Press; 2000.  
 [34] Lux T. Network theory is sorely required. Nature 2011;469:303–303.  
 [35] Malevergne Y, Sornette D. Extreme financial risks. From dependence to risk management. Berlin: Springer-Verlag; 2006.  
 [36] Mandelbrot B, Wallis J. Computer experiments with fractional gaussian noises. Water Resour Res 1969;5:228–67.  
 [37] Mantegna RN, Stanley HE. An Introduction to econophysics. Correlations and complexity in finance. Cambridge: Cambridge Univ. Press; 2000.  
 [38] Matia K, Yamasaki K. Statistical properties of demand fluctuation in the financial market. Quant Finance 2005;5(6):513–17.  
 [39] McSharry PE, Smith LA, Tarassenko L, Martinerie J, Quyen MLV, Baulc M, et al. Prediction of epileptic seizures: are nonlinear methods relevant? Nat Med, Lett Editor 2003;9(3):241–2.  
 [40] Metzler R, Klafter J. The random walk's guide to anomalous diffusion: a fractional dynamics approach. Phys Rep 2000;339:1–77.  
 [41] Plerou V, Gopikrishnan P, Stanley HE. Two phase behaviour of financial markets. Nature 2003;421:129–30.  
 [42] Plerou V, Gopikrishnan P, Stanley HE. Two phase behaviour and the distribution of volume. Quant Finance 2005;5:519–21.  
 [43] Potters M, Bouchaud J.-P. Comment on "two-phase behavior of financial markets. 2003. ArXiv:cond-mat/0304514v1.  
 [44] Preis T. Econophysics: complex correlations and trend switchings in financial time series. Eur Phys J ST 2011;194(1):5–86.  
 [45] Preis T, Schneider JJ, Stanley HE. Switching phenomena in financial markets. PNAS 2011;108(19):7674–8.  
 [46] Preis T, Stanley HE. Switching phenomena in a system with no switches. J Stat Phys 2010;138(1–3):431–46.  
 [47] Preis T, Stanley HE. Trend switching processes in financial markets. In: Takayasu M, Watanabe T, Takayasu H, editors. Econophysics approaches to large-scale business data and financial crisis. Tokyo: Springer-Verlag; 2010. p. 3–26.  
 [48] Preis T, Stanley HE. Bubble trouble. Phys World 2011;24:29–32.  
 [49] Preis T, Stanley HE. How to characterize trend switching processes in financial markets. Bull Asia Pacific Cent Theor Phys 2009;23:18–23.2009  
 [50] Roehner BM. Patterns of speculation. A Study observational econophysics. Cambridge: Cambridge Univ. Press; 2002.  
 [51] Rosser JB Jr. Implications for teaching macroeconomics of complex dynamics. Dept. Economics, James Madison Univ., Harrisonburg; 2004.  
 [52] Schadschneider A, Chowdhury D, Nishinari K. Stochastic transport in complex systems. From molecules to vehicles. Amsterdam: Elsevier; 2011.  
 [53] Scheffer M, Bascompte J, Brock WA, Brovkin V, Carpenter SR, Dakos V, et al. Early-warning signals for critical transitions. Nature 2009;461:53–9.  
 [54] Sornette D. Why stock markets crash. Princeton and Oxford: Princeton Univ. Press; 2003.  
 [55] Sornette D. Critical Phenomena in Natural Sciences. Chaos, fractals, selforganization and disorder: concepts and tools. Springer series in synergetics. 2nd ed. Heidelberg: Springer-Verlag; 2004.

- 932 [56] Nawrocki D, Vaga T. A bifurcation model of market returns. *Quant Finance* 2014;14(3):509–28. 945  
933 946  
934 [57] Sornette D. Dragon-kings, black swans and the prediction of crises. *Int J Ter- 947*  
935 *raspace Eng* 2009;2:1–17. 948  
936 [58] Stanley HE, Buldyrev SV, Franzese G, Havlin S, Mallamace F, Kumar P, et al. 949  
937 Correlated randomness and switching phenomena. *Physica A* 2010;389:2880– 950  
938 93. 951  
939 [59] Vandewalle N, Ausloos M, Boveroux P, Minguet A. Visualizing the log-periodic 952  
940 pattern before crashes. *Eur J Phys B* 1999;9:355–9. 953  
941 [60] van Kampen NG. *Stochastic processes in physics and chemistry*. Amsterdam: 954  
942 North-Holland; 1987. 955  
943 [61] Weiss GH. A primer of random walkology. In: Bunde A, Havlin S, editors. *Frac- 956*  
944 *tals in science*. Berlin: Springer-Verlag; 1985.
- [62] Weron R. Estimating long-range dependence: finite sample properties and confidence intervals. *Physica A* 2002;312:285–99.
- [63] Wissel C. A universal law of the characteristic return time near thresholds, 65. Berlin: Oecologia; 1984. p. 101–7.
- [64] Zeeman EC. On the unstable behavior of stock exchanges. *J Math Econ* 1974;39–49.
- [65] Zeeman EC. Catastrophe theory: selected papers, 1972–77. *Bull Amer Math Soc (N S)* 1978;84:1360–8. Errata, *Bull. Amer. Math. Soc. (N. S. )* 1, 681–681 (1979)
- [66] Zeeman EC. Evolution of catastrophe theory. *Understanding catastrophe*. Cambridge: Cambridge Univ. Press; 1992.
- [67] Zheng B, Qiu T, Ren F. Two-phase phenomena, minority games, and herding. *Phys Rev E* 2004;69(046115/1-6).